

# Lawrence Berkeley National Laboratory

## Recent Work

### Title

CALCULATION OF PARITY VIOLATING EFFECTS IN THE  $62P^-72P^-$  FORBIDDEN MI TRANSITION IN THALLIUM

### Permalink

<https://escholarship.org/uc/item/74p63865>

### Author

Neuffer, David V.

### Publication Date

1977

00004703150

Submitted to Physical Review A

LBL-6043

Preprint c. |

CALCULATION OF PARITY VIOLATING EFFECTS IN THE  
 $6^2P_{1/2} - 7^2P_{1/2}$  FORBIDDEN M1 TRANSITION IN THALLIUM

David V. Neuffer and Eugene D. Commins

RECEIVED  
LAWRENCE  
BERKELEY LABORATORY

January 1977

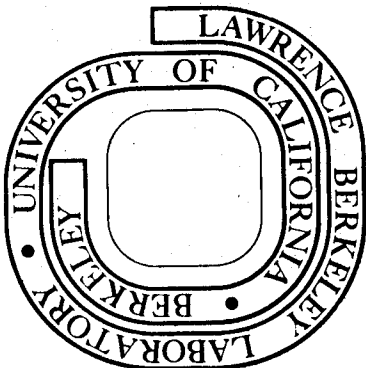
APR 22 1977

LIBRARY AND  
DOCUMENTS SECTION

Prepared for the U. S. Energy Research and  
Development Administration under Contract W-7405-ENG-48

**For Reference**

Not to be taken from this room



LBL-6043  
c. |

## **DISCLAIMER**

This document was prepared as an account of work sponsored by the United States Government. While this document is believed to contain correct information, neither the United States Government nor any agency thereof, nor the Regents of the University of California, nor any of their employees, makes any warranty, express or implied, or assumes any legal responsibility for the accuracy, completeness, or usefulness of any information, apparatus, product, or process disclosed, or represents that its use would not infringe privately owned rights. Reference herein to any specific commercial product, process, or service by its trade name, trademark, manufacturer, or otherwise, does not necessarily constitute or imply its endorsement, recommendation, or favoring by the United States Government or any agency thereof, or the Regents of the University of California. The views and opinions of authors expressed herein do not necessarily state or reflect those of the United States Government or any agency thereof or the Regents of the University of California.

Calculation of Parity Violating Effects

in the

$6^2P_{1/2} - 7^2P_{1/2}$  Forbidden M1 Transition in Thallium<sup>†\*</sup>

David V. Neuffer

and

Eugene D. Commins

Physics Department, University of California

Berkeley, California 94704

and

Materials and Molecular Research Division

Lawrence Berkeley Laboratory

Berkeley, California 94720

† Research supported by United States Energy Research and Development Administration.

\* To be submitted to Physical Review A.

ABSTRACT

Calculations are presented of the El amplitude expected in the  $6^2P_{1/2}-7^2P_{1/2}$  forbidden M1 transition in Tl if parity is violated in the neutral weak e-N interaction, as proposed in a number of gauge models, including that of Weinberg and Salam. Valence electron wave-functions are generated as numerical solutions to the Dirac equation in a modified Tietz central potential. These wave-functions are used to calculate allowed El oscillator strengths, hfs splittings, and Stark El transition amplitudes. These results are compared with experiment and the agreement is generally good. The relativistic  $6^2P_{1/2}-7^2P_{1/2}$  M1 transition amplitude  $\mathcal{M}$  is also calculated and corrections due to interconfiguration mixing, Breit interaction, and hfs mixing are included. The result:  $\mathcal{M}_{\text{theo}} = (-3.2 \pm 1.0) \cdot 10^{-5} \frac{|e|\hbar}{2m_e c}$  is in agreement with the experimental value:  $\mathcal{M}_{\text{expt}} = (-2.11 \pm 0.30) \cdot 10^{-5} \frac{|e|\hbar}{2m_e c}$ . The parity-violating El amplitude  $\mathcal{E}_{\text{PV}}$  is calculated and a value for the circular dichroism 
$$\delta \cong \frac{2\text{Im}(\mathcal{E}_{\text{PV, Theo}})}{\mathcal{M}_{\text{expt}}} = -2.6 \cdot 10^{-3}$$
 is obtained. Parity violating effects in other Tl transitions are discussed.

## INTRODUCTION

Discovery of strangeness-conserving neutral weak currents in neutrino-nucleon scattering experiments<sup>1</sup> has stimulated considerable interest in the possible existence of a weak neutral electron-nucleon interaction. If such an interaction violates parity, as predicted by several theoretical gauge models including that of Weinberg and Salam<sup>2</sup> (W-S), effects in heavy atoms such as optical rotation in allowed M1 transitions, and circular dichroism (dependence of absorption on photon helicity) in forbidden M1 transitions may be observable.

An experiment to study the latter effect in the doubly forbidden M1 transition  $6^2P_{1/2} - 7^2P_{1/2}$  (292.7 nm.) in atomic Tl vapor has been proposed.<sup>3</sup> The idea, originally suggested for the  $6^2S_{1/2} - 7^2S_{1/2}$  transition in Cs by Bouchiat and Bouchiat,<sup>4</sup> is that a short range, parity violating, neutral weak interaction  $H_{PV}$  mixes the  $6^2P_{1/2}, 7^2P_{1/2}$  Tl states with  $n^2S_{1/2}$  states. Thus the transition  $6^2P_{1/2} - 7^2P_{1/2}$ , nominally M1 with amplitude

$$\mathcal{M} = \langle 7^2P_{1/2}, m_J | M1 | 6^2P_{1/2}, m_J \rangle \quad (1)$$

also contains a parity-violating electric dipole component with amplitude  $\mathcal{E}_{PV} = \langle 7^2P_{1/2}, m_J | E1 | 6^2P_{1/2}, m_J \rangle$ . It can be shown that interference between  $\mathcal{M}$  and  $\mathcal{E}_{PV}$  results in a dependence of the  $6^2P_{1/2} - 7^2P_{1/2}$  absorption rate  $W$  on right (R) or left (L) handed photon helicity:

$$\delta = \frac{W(R) - W(L)}{W(R) + W(L)} = 2 \frac{\text{Im}(\mathcal{E}_{PV}) \cdot \mathcal{M}}{|\mathcal{M}|^2 + |\mathcal{E}_{PV}|^2} \approx \frac{2 \text{Im}(\mathcal{E}_{PV})}{\mathcal{M}} \quad (2)$$

The "circular dichroism"  $\delta$  can be detected by observing the fluorescence accompanying decay of the  $7^2P_{1/2}$  state (see Fig. 1). The first step in

that experiment was the determination of the M1 amplitude itself, the result being:<sup>3</sup>

$$\mathcal{M}_{\text{expt}} = (-2.11 \pm 0.30) \cdot 10^{-5} \mu_B \quad (3)$$

where  $\mu_B = |e|\hbar/2m_e c$ . In that measurement and also in the experiment proposed to detect  $\delta$ , use is made of the interference which occurs between  $\mathcal{M}$  and/or  $\mathcal{E}_{\text{PV}}$  and the Stark-induced electric dipole amplitude  $\mathcal{E}_S$  for  $6^2P_{1/2} - 7^2P_{1/2}$  transitions in an external electric field.

In this paper we present results of calculations of the atomic structure of Tl which are necessary in order to make useful comparisons between these experiments and the predictions of models of the neutral weak interaction. The thallium atom has 81 electrons with a ground state electronic configuration:  $1s^2 \dots 5d^{10} 6s^2 6p$ . Our approach is to assume that all singly-excited TlI states of interest have the same inner electron configuration ( $1s^2 \dots 5d^{10} 6s^2$ , with total  $L=0$ ,  $S=0$ ) as that of the ground state, and differ only in the valence electron orbital. This approximation, while not strictly correct, is reasonable, since inner shell ionization energies are at least several times larger than that of the 6p valence electron. It also has the obvious virtue of simplicity, since within such an approximation most properties of interest to us can be calculated from the valence electron wave-function, which is obtained by solving the Dirac equation numerically in a spherically symmetric potential, for all states of interest. We have chosen the potential:

$$V(r) = -\frac{e^2(Z-1)}{r(1+\eta r)^2} e^{-\gamma r} - \frac{e^2}{r} \quad (4)$$

Without the exponential shielding factor  $e^{-\gamma r}$ ,  $V(r)$  is the "Tietz" potential,<sup>5</sup> which yields a good approximate solution to the Thomas-Fermi equation. The factor  $e^{-\gamma r}$  is inserted to account for the exponential decrease of electron density for large  $r$ . Parameters  $\eta$  and  $\gamma$  are chosen so that the calculated and observed  $6^2P_{1/2}$  and  $7^2P_{1/2}$  energies agree.

We describe calculations of energy levels, allowed E1 oscillator strengths, and  $P_{1/2}$ ,  $S_{1/2}$  hyperfine structure splittings, all in good agreement with observations (see Sec. 2). As is well known, the  $6^2P_{3/2}$  hfs splitting is strongly affected by interconfiguration interaction, and a correction for this must be applied in order to obtain reasonable agreement with experiment (see Appendix A). Our calculation of  $\mathcal{M}$  (Sec. 3) includes the one-electron relativistic contribution and corrections due to interconfiguration, hyperfine, and Breit interactions; the result is in agreement with the experimental value (Eq. 3). Our calculation of the Stark transition amplitudes  $\mathcal{E}_S$  yields two second-order matrix elements  $\alpha, \beta$  for linearly polarized excitation light parallel and perpendicular, respectively, to the applied static field  $E$ . The ratio  $\beta/\alpha$  is in agreement with the experimental results of Chu, Commins, and Conti<sup>3</sup> (see Sec. 5).

The satisfactory agreement between experiment and the calculations described in the previous paragraph provide confidence that our estimate of the parity violating amplitude  $\mathcal{E}_{PV}$  should be reliable enough



so that future experimental determinations of circular dichroism may yield useful tests of gauge models. For purposes of the present discussion we present the analysis in terms of the W-S model,<sup>2</sup> which describes low-energy strangeness conserving neutral weak interactions in terms of an effective Hamiltonian density:

$$\mathcal{H}(x) = \frac{G}{\sqrt{2}} J_\lambda(x) \cdot J^\lambda(x) \quad (5)$$

where G is the Fermi coupling constant of weak interactions

$G = 3 \times 10^{-12}$  in units ( $\hbar = m_e = c = 1$ ) used throughout. The current  $J^\lambda(x)$  has both hadronic and leptonic parts, the former being expressible as:

$$J_{\text{had}}^\lambda = V^{\lambda,0} + A^{\lambda,0} - 2 \sin^2 \theta_w J^{\lambda,EM} \quad (6)$$

where  $V^{\lambda,0}$  is the  $I_3$  component of the strangeness-conserving hadronic vector current,  $A^{\lambda,0}$  is the neutral  $\Delta S=0$  hadronic axial current,  $J^{\lambda,EM}$  is the EM current, and  $\theta_w$  is the so-called "Weinberg" angle, which is given by  $\sin^2 \theta_w \cong 0.3$ . That portion of the neutral leptonic current involving  $e^-$  is:

$$J_\lambda^{\text{lept},e^-} = -\frac{1}{2} \left[ (1 - 4\sin^2 \theta_w) \bar{\Psi}_e \gamma_\lambda \Psi_e + \bar{\Psi}_e \gamma_\lambda \gamma_5 \Psi_e \right] \quad (7)$$

where  $\Psi_e$  is the electron field operator.

The first and second terms on RHS are respectively vector and axial-vector currents. We are interested in those portions of  $\mathcal{H}(x)$  which are pseudoscalar, not scalar; thus we consider the product of the axial portion of  $J_\lambda^{\text{lept},e^-}$  and the vector portion of  $J_{\text{had}}^\lambda$ . (The other pseudoscalar term corresponding to the product of the vector part of  $J_\lambda^{\text{lept},e^-}$  and the axial part of  $J_{\text{had}}^\lambda$  gives a much smaller contribution since it is

proportional to total nuclear spin, and for a heavy nucleus, most of the nucleon spins cancel in pairs.) Ignoring this latter portion, we find:

$$\mathcal{H}^{PV}(x) \cong -\frac{G}{\sqrt{2}} \bar{\psi}_e \gamma_\lambda \gamma_5 \psi_e \cdot (V^{\lambda,0} - 2\sin^2\theta_w J^{\lambda,EM}) \quad (8)$$

Taking matrix elements of  $\mathcal{H}^{PV}(x)$  for the static limit of the nucleus, we obtain the matrix element of the effective Hamiltonian:

$$\langle H^{PV} \rangle = \frac{-G}{2\sqrt{2}} \psi_2^*(\vec{x}) \gamma_5 \psi_1(\vec{x}) \Big|_{x=0} \quad (9)$$

where

$$Q_w = (1-4\sin^2\theta_w) Z - N \quad (10)$$

and  $\psi_1(\vec{x})$ ,  $\psi_2(\vec{x})$  are Dirac wave-functions corresponding to states of opposite parity, and "x=0" indicates the product is averaged over the nuclear volume. In fact only  $P_{1/2}$  and  $S_{1/2}$  states yield non-negligible matrix elements. Equation (9) is derived from the W-S model. However, other gauge models with parity violation would lead to the same expression with only  $Q_w$  of Eq. 10 being model dependent. In most cases  $|Q_w| \sim Z$ . In Sec. 4 we use Eq. (9) to calculate  $\epsilon_{PV}$ . Finally, Sec. 6 contains an estimate of parity violating effects for transitions in Tl other than  $6^2P_{1/2} - 7^2P_{1/2}$ .

## 2. THALLIUM WAVE FUNCTIONS IN THE ONE ELECTRON

### CENTRAL FIELD APPROXIMATION

#### 2.1 Construction of Wave Functions

The Dirac equation is

$$[\vec{\alpha} \cdot \vec{p} + \beta - eV]\psi = (1 - E_I)\psi \quad (11)$$

where  $E_I$  is the valence electron ionization energy [(1- $E_I$ ) is the total electron energy including rest mass], and  $\vec{\alpha}$  and  $\beta$  are the usual Dirac

matrices. We write

$$\psi = \begin{pmatrix} \frac{f(r)}{r} \chi_{\kappa}^{\mu} \\ i \frac{g(r)}{r} \chi_{-\kappa}^{\mu} \end{pmatrix} \quad (12)$$

As usual,  $\kappa = \mp(j + \frac{1}{2})$  for even(odd) parity states, the  $\chi_{\pm\kappa}^{\mu}$  are two-component angular momentum-spin functions<sup>6</sup> given by:

$$\chi_{\kappa}^{\mu}(\theta, \phi) = \begin{pmatrix} C(\frac{1}{2}, \ell, j; \frac{1}{2}, \mu - \frac{1}{2}, \mu) Y_{\ell}^{\mu - \frac{1}{2}}(\theta, \phi) \\ C(\frac{1}{2}, \ell, j; -\frac{1}{2}, \mu + \frac{1}{2}, \mu) Y_{\ell}^{\mu + \frac{1}{2}}(\theta, \phi) \end{pmatrix} \quad (13)$$

the C's are Clebsch - Gordan coefficients,  $\mu \equiv m_j$ ,  $\ell = |\kappa + 1/2| - 1$ , and the Y's are spherical harmonics. Equation (12) reduces to the two coupled radial equations:

$$\begin{aligned} \frac{df}{dr} &= -\frac{\kappa}{r} f + [2 - E_1 - V(r)]g \\ \frac{dg}{dr} &= \frac{\kappa}{r} g + [E_1 + V(r)]f \end{aligned} \quad (14)$$

Following the procedure used by Schwartz<sup>7</sup> to calculate hyperfine structure splittings in Tl and other heavy atoms, we choose for  $V(r)$  the modified Tietz potential of Eq. (4). Parameters  $\eta$  and  $\gamma$  are chosen so that calculated and observed  $6^2P_{\frac{1}{2}}$  and  $7^2P_{\frac{1}{2}}$  energies agree. The fitting procedure is as follows:

(1) For very small  $r$  ( $r \leq r_0 = .02 \frac{\hbar}{m_e c} = .02$ ) i.e. for  $r$  within the nuclear radius  $r_0$ , one of the following three potentials is chosen:

$$a) \quad V(r) = \frac{-Ze^2}{r} \quad (\text{Point nucleus})$$

$$b) \quad V(r) = \frac{-Ze^2}{r_0} \quad (\text{Constant potential})$$

$$c) \quad V(r) = \frac{Ze^2}{2r_0} \left( \frac{r^2}{r_0^2} - 3 \right) \quad (\text{Constant nuclear charge density})$$

The initial wave-function values for this region are generated using a power series expansion to solve Eq. (14).

(2) For  $r \geq r_0$  Eqs. (14) for  $f(r)$ ,  $g(r)$  are integrated numerically stepwise using a fourth order Runge-Kutta method.<sup>8</sup> Approximately 5000 intervals of length increasing from  $.001 \lambda$  to  $2.0 \lambda$  are used.

(3) The eigenvalue condition is that

$\lim_{r \rightarrow \infty} f(r) = 0$ . The energy  $E_I$  in Eqs. (14) is varied to insure that this condition is satisfied.

The energy spectrum does not depend strongly on the choice of potential in step (1). Of all the quantities computed below, only the weak electron-nucleus interaction depends significantly on this choice, and for that quantity the dependence is only  $\sim 10\%$ . The number of intervals can be reduced substantially without significant loss of precision except for calculation of the forbidden M1 transition (see Sec. 3); however this reduction would provide no economic advantage on the LBL CDC 7600 computer. The calculation procedure can be reversed by

choosing an asymptotic form for  $f$  and  $g$  at large  $r$ , and integrating step-wise toward  $r = 0$ . This yields the same states as the procedure actually used, but is less convenient for calculation of  $\epsilon_{PV}$ .

The values of  $\eta$  and  $\gamma$  chosen for most calculations are -

$$\begin{aligned}\eta &= 2.5937a_0^{-1} = 355.43 \lambda^{-1} \\ \gamma &= .2579a_0^{-1} = 35.34 \lambda^{-1}\end{aligned}\tag{15}$$

Numerical values of  $\frac{f}{r}$  and  $\frac{g}{r}$  vs  $r$  are given for several states in Table I. These values are chosen to yield agreement between calculated and observed  $6^2P_{1/2}$ ,  $7^2P_{1/2}$  energy levels to within 0.1%. Other low lying  $S_{1/2}$ ,  $D_{1/2}$ ,  $P_{1/2}$ , and  $P_{3/2}$  energy levels are calculated, and these all agree with observations to within 2%. Table II includes a comparison of calculated and observed energy levels.

## 2.2 Hyperfine Structure

The one-electron central-field (OECF) wave functions described above can be used to calculate hyperfine structure splittings for comparison with experimental values. This comparison provides a reasonably sensitive test of the accuracy of calculations of  $\epsilon_{PV}$  since both the latter and the hfs depend on values of the wave-functions near the origin. The perturbation Hamiltonian for hfs is

$$H_{HFS} = e\vec{\alpha} \cdot \vec{A} = e\vec{\alpha} \cdot \frac{\vec{m}_n \times \vec{r}}{r^3} = e \vec{m}_n \cdot \frac{\vec{r} \times \vec{\alpha}}{r^3}\tag{16}$$

where  $\vec{m}_n = g_n \mu_n \vec{I}$  is the nuclear magnetic moment operator,  $\mu_n$  is the nuclear Bohr magneton, and  $I = \frac{1}{2}$  is the spin for both stable thallium isotopes,  $^{203}\text{Tl}$  and  $^{205}\text{Tl}$ . Also  $g_n(^{203}\text{Tl}) = 3.223$ ,  $g_n(^{205}\text{Tl}) = 3.255$ ;<sup>9</sup>

in our calculations these are averaged to  $g_n = 3.24$ . It can then be shown that the hfs energy splittings are given in first-order by:<sup>6</sup>

$$\Delta W = e g_n \mu_n (J + \frac{1}{2}) \cdot \frac{8\kappa}{4\kappa^2 - 1} \cdot R \quad (17)$$

where

$$R = \int_0^\infty \frac{f g}{r^2} dr \quad (18)$$

Table II includes a list of hfs splittings calculated for the various energy levels, together with experimental values where these are available. The discrepancies are not due to major defects in the wave functions, but rather to interconfiguration interaction, which is known to have an especially large effect on the  $6^2P_{3/2}$  state. This is demonstrated in Appendix A which contains an estimate of interconfiguration interaction for 6p electron states. Although the effect on the  $6^2P_{3/2}$  hfs splitting is large it can be shown that interconfiguration interaction corrections to  $\epsilon_{PV}$  are negligible.

### 2.3 Fine Structure

Another test of the wave-function for small  $r$  is the fine structure splitting  $\Delta E = E(j = \ell + \frac{1}{2}) - E(j = \ell - \frac{1}{2})$  for  $\ell \neq 0$ . Non-relativistically,

$$\Delta E = (\ell + \frac{1}{2}) \langle n\ell | \frac{1}{r} \frac{dV}{dr} | n\ell \rangle$$

In a relativistic calculation such as ours, the fine structure is part of the unperturbed Hamiltonian, and the calculated fine structure is simply the difference between calculated  $(j = \ell + \frac{1}{2})$  and  $(j = \ell - \frac{1}{2})$  energy levels. Comparison of these differences with observed energy differences from Table II for P states yields discrepancies  $\leq 10\%$ .

### 2.4 Allowed Electric Dipole Transitions

We also calculate electric dipole radial integrals and transition strengths using the OECF wave-functions. In the relativistic notation of Berestetskii, Lifschitz, and Pitaevskii,<sup>10</sup> the transition matrix element is

$$V_{fi} = e \int d^3\vec{r} j_{fi}^\mu(\vec{r}) A_\mu^*(\vec{r}) \quad (19)$$

where  $j_{fi}^\mu(\vec{r}) = \bar{\psi}_f \gamma^\mu \psi_i$  is written in terms of the initial and final Dirac wave-functions  $\psi_i, \psi_f$ ,  $\gamma^\mu$  are the standard 4x4 matrices, and  $A_\mu(\vec{r})$  is the 4-vector potential. In the long-wavelength approximation for an electric multipole field of order J,M we have:

$$A_\mu(\vec{r}) = (A_0(\vec{r}), 0, 0, 0)$$

$$\begin{aligned} A_0(\vec{r}) &= - \int \frac{d^3\vec{k}}{(2\pi)^3} \sqrt{\frac{J+1}{J}} \frac{4\pi^2}{\omega^{3/2}} \delta(|\vec{k}| - \omega) Y_J^M\left(\frac{\vec{k}}{\omega}\right) \cdot e^{i\vec{k}\cdot\vec{r}} \\ &\cong r^J (-1)^{M+1} i^J \sqrt{\frac{J+1}{J}} \frac{2\omega^{J+1/2}}{(2J+1)!!} Y_J^M\left(\frac{\vec{r}}{r}\right) \end{aligned} \quad (20)$$

For E1 radiation, this becomes:

$$A_0(\vec{r}) = (-1)^{M+1} \cdot i \cdot r \cdot \frac{2\sqrt{2}}{3} \omega^{3/2} Y_1^M\left(\frac{\vec{r}}{r}\right) \quad (21)$$

Combining Eqs. (19) and (21) we obtain:

$$V_{fi}^{1,M} = (-1)^i \omega^{3/2} \frac{2\sqrt{2}}{3} \int d^3\vec{r} \psi_f^* (\vec{r}) r Y_1^{M*} \left( \frac{\vec{r}}{r} \right) \psi_i (\vec{r}) \quad (22)$$

The spontaneous emission rate A is given by:

$$A_{fi} = 2\pi \overline{V_{fi}^2}$$

where  $\overline{V_{fi}^2}$  is  $V_{fi}^2$  summed over photon states and final electron states  $(j_f, m_f)$ , and averaged over initial electron states  $(j_i, m_i)$ . For OECF wave-functions the angular integration is easily separated and we find the following:

Transition	A-coefficient
$S_{\frac{1}{2}} \rightarrow P_{\frac{1}{2}}, D_{3/2} \rightarrow P_{\frac{1}{2}}$	$4/9 e^2 \omega^3 \langle r \rangle_{fi}^2$
$S_{\frac{1}{2}} \rightarrow P_{3/2}$	$8/9 e^2 \omega^3 \langle r \rangle_{fi}^2$
$D_{3/2} \rightarrow P_{3/2}$	$4/45 e^2 \omega^3 \langle r \rangle_{fi}^2$
$D_{5/2} \rightarrow P_{3/2}$	$8/15 e^2 \omega^3 \langle r \rangle_{fi}^2$

where  $\omega$  is the observed energy difference between initial and final states, and  $\langle r \rangle_{fi} = \int r (f_f f_i + g_f g_i) dr$ . The signs of these radial integrals are fixed by the convention that  $f(r) > 0$  as  $r \rightarrow 0$  for every state. In Table III, the radial integrals  $\langle r \rangle_{fi}$  and calculated A-coefficients for  $nD \rightarrow 6P$  and  $nS \rightarrow 6P$  transitions are listed, together with observed A coefficients for the same transitions as determined by Gallagher and Lurio.<sup>11</sup> The agreement between theory and experiment is generally good, the discrepancy in the transition rates typically being  $\leq 20\%$ . This corresponds to a discrepancy in the



radial integrals of  $\lesssim 10\%$ , and reveals that our wave functions are reasonably accurate in the range  $r \geq 2\text{\AA}$ .

The oscillator strengths  $F_{fi}$  are defined by

$$F_{fi} = \left( \frac{2J_f + 1}{2J_i + 1} \right) \frac{A_{if}}{2e^2 \omega^2} \quad (23)$$

where  $J_i, J_f$  are the initial and final total electronic angular momenta. These quantities have previously been calculated by Anderson et al.<sup>12</sup> by a method similar to ours (one-electron Dirac wave-function and central potential). Table III includes a comparison of their calculated oscillator strengths with ours for  $nD \rightarrow 6P$  and  $nS \rightarrow 6P$  transitions. Table IV gives the same comparison for  $7P \rightarrow nS$  and  $7P \rightarrow nD$  transitions, the radial integrals for which are needed in evaluation of  $\mathcal{E}_{PV}$  and  $\mathcal{E}_S$  (see Secs. 4 and 5). Our calculated oscillator strengths and those of Anderson et al. are nearly identical, which suggests that the discrepancies ( $\lesssim 20\%$ ) between calculated and observed values are due to a failure of the OECF approximation, rather than merely to an inadequate central potential. Thus to obtain more accurate results it may be necessary to go beyond the simple OECF model.

### 3. MAGNETIC DIPOLE TRANSITION RATES

#### 3.1 The Relativistic Contribution

The relativistic contribution to  $M$  arises from the transition matrix element:<sup>10</sup>

$$V_{fi} = i e \sqrt{2\omega} \int d^3r \psi_f^*(\vec{r}) \vec{\alpha} \psi_i(\vec{r}) \cdot \left[ \frac{\vec{r} \times \vec{\nabla}}{\sqrt{2}} Y_{lm}^* \right] g_1(kr) \quad (24)$$

where  $g_1(kr) = \sqrt{\frac{\pi}{2kr}} J_{3/2}(kr)$  is a spherical Bessel function. Using Eq. (12) for  $\psi_i, \psi_f$  which are both  $P_{1/2}$  states, employing  $\vec{\alpha} = \begin{pmatrix} 0 & \vec{\sigma} \\ \vec{\sigma} & 0 \end{pmatrix}$  and  $(\vec{\sigma} \cdot \vec{r}/r)\chi_1^\mu = -\chi_{-1}^\mu$ , and utilizing the anti-commutation of  $\vec{\sigma} \cdot \vec{r}/r$  and  $\vec{\sigma} \cdot \vec{\nabla} Y_{lm}$ , we obtain:

$$V_{fi} = -ie\sqrt{2\omega} \int dr g_1(kr) (f_f g_i + f_i g_f) \cdot \int r d\Omega \chi_{-1}^{\mu_f*} \vec{\sigma} \cdot \vec{\nabla} Y_{lm}^* \chi_{-1}^{\mu_i} \quad (25)$$

We rewrite this as

$$V_{fi} = (-1)^m i\sqrt{2/3}\pi \omega^{3/2} \vec{\mu}_{fi} \cdot \hat{\epsilon}_m \quad (26)$$

where  $\hat{\epsilon}_m$  is the spherical unit vector:

$$\hat{\epsilon}_m = \vec{\nabla} (\sqrt{4\pi/3} r Y_{1m}) \quad (27)$$

and

$$\vec{\mu}_{fi} \cdot \hat{\epsilon}_m = -e \int dr g_1(kr) \frac{1}{\omega} (f_f g_i + g_f f_i) \cdot \int d\Omega \chi_{-1}^{\mu_f*} \vec{\sigma} \cdot \vec{\nabla} \sqrt{4\pi/3} r Y_{1m} \chi_{-1}^{\mu_i} \quad (28)$$

for  $P_{1/2} \rightarrow P_{1/2}$  transitions. The expression for  $\vec{\mu}_{fi} \cdot \hat{\epsilon}_m$  in the case of  $S_{1/2} - S_{1/2}$  transitions is the same except for a change in sign.

To find the transition rate

$$A = 2\pi \overline{|V_{fi}|^2} = \frac{4}{3} \omega^3 \overline{|\vec{\mu}_{fi} \cdot \hat{\epsilon}_m|^2} \quad (29)$$

we sum over final and average over initial states to obtain:

$$A = 4\omega^3 e^2 \left| \int \frac{g_1(kr)}{\omega} (f_f g_i + g_f f_i) dr \right|^2 \quad (30)$$

This formula was previously obtained by Johnson<sup>13</sup> for the  $2^2S_{1/2} - 1^2S_{1/2}$  M1 transition in hydrogen. The result is also valid for allowed  $\frac{1}{2} - \frac{1}{2}$  transitions. In this case  $\vec{\mu}_{fi}$  of Eq. (28) approaches the familiar

$$\vec{\mu}_{fi} = \int \psi_f^* \left[ \frac{e}{2} \vec{L} + \mu_e \frac{\vec{S}}{S} \right] \psi_i d^3r \quad (31)$$

in the non-relativistic limit. This expression vanishes if the radial parts of  $\psi_i$  and  $\psi_f$  are orthogonal.

We use our OECF radial wave-functions for  $6^2P_{1/2}$ ,  $7^2P_{1/2}$  states to compute the result:

$$\mathcal{M}_{REL} = -e \int \frac{g_1(kr)}{\omega} (f_i g_f + g_i f_f) dr = -1.757 \times 10^{-5} \mu_B \quad (32)$$

The extremely small size of this matrix element implies that relatively large corrections might occur due to interconfiguration mixing, hyperfine mixing, and the Breit interaction.

### 3.2 Interconfiguration Interaction Correction

Electrostatic interaction of the outer electron with excited core states alone (as in Appendix A) does not directly effect the M1 transition rate, since it mixes only those states having the same total L and S ( $^2P_{1/2}$  in Tl).<sup>14</sup> However, in second order, Spin-orbit coupling allows an admixture of different L, S atomic states (e.g.  $^4P_{1/2}$  in Tl) and this admixture can give rise to a finite M1 amplitude — even in the non-relativistic limit.

A consistent fourth order treatment is necessary; the calculation which follows is similar to that done by Phillips for corrections to  $g_J(\text{Cs})$ .<sup>14</sup> Since the ground configuration of Tl is  $(1s^2 \dots 5d^{10} 6s^2 6p)$ ,

we only consider the effects of 6s-electron excitation (the correction due to 5d excitation turns out to be smaller). The unperturbed states are

$$\begin{aligned}\psi_6 &\equiv \psi(6^2P_{1/2}) = 6s^2(^1S_0) 6p^2P_{1/2} \\ \psi_7 &\equiv \psi(7^2P_{1/2}) = 6s^2(^1S_0) 7p^2P_{1/2}\end{aligned}\quad (33)$$

The first-order perturbation is the electrostatic interaction and the perturbing states considered are:

$$\begin{aligned}\phi_6 &= 6s7s(^3S_1) 6p^2P_{1/2} \\ \phi_7 &= 6s7s(^3S_1) 7p^2P_{1/2}\end{aligned}\quad (34)$$

Thus the perturbed states are

$$\begin{aligned}\psi'_6 &= \psi_6 + \alpha_6\phi_6 + \alpha_7\phi_7 \\ \psi'_7 &= \psi_7 + \beta_6\phi_6 + \beta_7\phi_7\end{aligned}\quad (35)$$

where  $\alpha_6$ ,  $\alpha_7$ ,  $\beta_6$ ,  $\beta_7$  are calculated by first order perturbation theory, and antisymmetrization of the total wave function is taken into account.

For example:

$$\alpha_6 = -\sqrt{3/2} \frac{G_1(6s, 6p; 7s, 6p)}{\Delta E}$$

where  $G_1(6s, 6p; 7s, 6p)$  is the exchange electrostatic integral,  $\Delta E = E(\phi_6) - E(\psi_6)$ , and  $E(\phi_6)$  is a fictitious energy calculated for a 6s7s6p configuration in the potential of Eq. (4). Numerical computation gives:

$$\alpha_6 = -.010, \alpha_7 = +.023, \beta_6 = .094, \beta_7 = .006. \quad (36)$$

The  $6s7s(^3S_1) np^2P_{1/2}$  states are now mixed with states

$$\phi'_n(^4P_{1/2}) = 6s7s(^3S_1) n'p^4P_{1/2} \quad (37)$$

by spin-orbit interaction. We employ the perturbation Hamiltonian

$$H' = \sum_i \xi_i \cdot \vec{L}_i \cdot \vec{S}_i = \frac{1}{2} \sum_i \left( \frac{1}{r} \frac{\partial V}{\partial r} \right)_i \vec{L}_i \cdot \vec{S}_i \quad (38)$$

and rewrite our wave functions as:

$$\begin{aligned} \psi'_6 = \psi_6 + \alpha_6 [\phi_6 + a_6 \phi'_6(^4P_{1/2}) + a_7 \phi'_7(^4P_{1/2})] \\ + \beta_6 [\phi_7 + b_6 \phi'_6(^4P_{1/2}) + b_7 \phi'_7(^4P_{1/2})] \end{aligned} \quad (39)$$

and

$$\begin{aligned} \psi'_7 = \psi_7 + \alpha_7 [\phi_6 + c_6 \phi'_6(^4P_{1/2}) + c_7 \phi'_7(^4P_{1/2})] \\ + \beta_7 [\phi_7 + d_6 \phi'_6(^4P_{1/2}) + d_7 \phi'_7(^4P_{1/2})] \end{aligned} \quad (40)$$

The coefficients  $a_6, \dots, d_7$  are calculated from the observed P-state fine structure splitting. For example,

$$a_6 = -\frac{2\sqrt{2}}{9} \cdot \frac{[E(6^2P_{3/2}) - E(6^2P_{1/2})]}{\Delta E} \quad (41)$$

where  $\Delta E = E(\psi_6) - E(\phi'_6)$ . We find:  $a_6 = +.033$ ,  $a_7 = +.0081$ ,  $b_6 = +.012$ ,  $b_7 = +.0029$ ,  $c_6 = +.061$ ,  $c_7 = +.012$ ,  $d_6 = +.022$ ,  $d_7 = .0043$ . The interconfiguration interaction correction to  $\mathcal{M}$  is now computed from Eqs. (39), (40) by means of the formula

$$\mathcal{M}_{II} = \langle \psi'_6 | M | \psi'_7 \rangle - \mathcal{M}_{REL} \quad (42)$$

In the evaluation of all the perturbing terms we use the non-relativistic form (31). We find:

$$\mathcal{M}_{II} = [(\alpha_7 c_6 + \beta_7 d_6)(\alpha_6 a_6 + \beta_6 b_6) + (\alpha_7 c_7 + \beta_7 d_7)(\alpha_6 a_7 + \beta_6 b_7)] \cdot \frac{1}{2} [g({}^4P_{1/2}) - g({}^2P_{1/2})] \cdot \frac{e}{2} = -1.9 \times 10^{-6} \mu_B \quad (43)$$

Inclusion of higher s-state excitations (6s ns np) does not significantly change Eq. (43). However, since the electrostatic exchange integrals are fairly sensitive to small changes in wave-functions, the 4th order result (43) might be in error by as much as a factor of 2.

### 3.3 Breit Interaction Corrections

The OECF approximation used up to now does not include a complete description of electron-electron interactions, even if we assume a spherically symmetric core. To order  $v^2/c^2$ , the electron-electron interaction contributes a term to the Hamiltonian:

$$\Delta H = \sum_{i < k} \frac{e^2}{r_{ik}} - \frac{e^2}{2} \sum_{i < k} \left( \frac{\vec{\alpha}_i \cdot \vec{\alpha}_k}{r_{ik}} + \frac{(\vec{\alpha}_i \cdot \vec{r}_{ik})(\vec{\alpha}_k \cdot \vec{r}_{ik})}{r_{ik}^3} \right) \quad (44)$$

The first term on RHS of (44) is in fact partially included in the central potential (Eq. 4) but the second term is not, and must be regarded as an additional perturbation. This term may be reduced to the following expression (Breit interaction)<sup>15</sup>:

$$\Delta H_B = \frac{e^2}{2} \sum_{i \neq k} [\vec{\nabla}_i \frac{1}{r_{ik}} \times \vec{p}_i] \cdot \vec{\sigma}_k - \frac{e^2}{2} \sum_{i < k} \left[ \frac{1}{r_{ik}} \vec{p}_i \cdot \vec{p}_k + \frac{1}{r_{ik}^3} (\vec{r}_{ik} \cdot (\vec{r}_{ik} \cdot \vec{p}_i)) \cdot \vec{p}_k \right] \quad (45)$$

In order to calculate the contribution of this interaction to the M1 transition we replace  $\vec{p}$  by  $\vec{p} + e\vec{A}$  (electron charge =  $-e$ ), where  $\vec{A} = \frac{\vec{B} \times \vec{r}}{2}$ .

Thus we obtain:

$$\Delta H_{B, \text{eff}} = \frac{e^3}{2} \sum_{i \neq k} (\vec{\nabla}_i \cdot \frac{1}{r_{ik}} \times \vec{A}_i) \cdot \vec{\sigma}_k - \frac{e^3}{2} \sum_{i \neq k} \left[ \frac{\vec{A}_i \cdot \vec{p}_k}{r_{ik}} + \frac{\vec{r}_{ik} \cdot \vec{A}_i}{r_{ik}^3} \frac{\vec{r}_{ik} \cdot \vec{p}_k}{r_{ik}^3} \right] \quad (46)$$

This expression has been derived previously by Abragam and Van Vleck,<sup>16</sup> and Schwartz.<sup>17</sup> We now consider the special case of one electron outside a spherically symmetric electron distribution; it has been shown that only electrons outside of closed shells give non-vanishing contributions.<sup>16</sup>

It can then be shown that the matrix element of the first term on RHS of (46), called the "Lamb" correction,<sup>18</sup> is:

$$\mathcal{M}_L = -\frac{e^3}{2} \int \psi_1'^* (\vec{r}_1) \vec{\sigma}_1 \cdot \vec{\nabla}_1 \times \left[ \int \frac{\vec{A}(\vec{r}_2) \rho(\vec{r}_2) d\tau_2}{|\vec{r}_1 - \vec{r}_2|} \right] \psi_1 (\vec{r}_1) d\tau_1 \quad (47)$$

where  $\rho(\vec{r}_2) = \sum_{k \neq 1} \psi_k^* (\vec{r}_2) \psi_k (\vec{r}_2)$

For present purposes we choose  $\psi_1, \psi_1'$  to be  $6P_{\frac{1}{2}}, 7P_{\frac{1}{2}}$  wave functions, respectively; for  $\rho(\vec{r}_2)$  we insert the spherically symmetric density obtained from our central potential, and we set  $\vec{B} \parallel z$ . Then the amplitude for the  $m_J = \frac{1}{2} \rightarrow m_J = \frac{1}{2}$  transition is reduced to a sum of radial integrals:

$$\mathcal{M}_L = \frac{e}{2} B \left[ -\frac{4e^2}{45} \langle V \rangle + \frac{e^2}{9} \langle W \rangle \right] \quad (48)$$

where

$$\langle V \rangle = \int_0^\infty \frac{F(r_1)}{r_1^3} \left[ \int_0^{r_1} r_2^4 \rho(r_2) dr_2 \right] F'(r_1) r_1^2 dr_1 \quad (49)$$

and

$$\langle W \rangle = \int_0^\infty F(r_1) \left[ \int_{r_1}^\infty \rho(r_2) r_2 dr_2 \right] F'(r_1) r_1^2 dr_1 \quad (50)$$

and  $F, F'$  are the non-relativistic 6p, 7p radial wave-functions, respectively. The resulting contribution to  $\mathcal{M}$  is evaluated numerically to be

$$\mathcal{M}_L = -4 \times 10^{-7} \mu_B \quad (51)$$

The second term on RHS of (46), called the "orbit-orbit" correction,<sup>16</sup> gives the following matrix element:

$$\begin{aligned} \mathcal{M}_{OR} = & \frac{-e^3}{6} \int \psi_1^*(\vec{r}_1) \left[ \frac{1}{r_1^3} \int_0^{r_1} \rho(r_2) r_2^4 dr_2 \right. \\ & \left. + \int_{r_1}^\infty \rho(r_2) r_2 dr_2 \right] \vec{L}_1 \cdot \vec{B} \psi_1'(\vec{r}_1) d^3r_1 \end{aligned} \quad (52)$$

For  $\vec{B} \parallel \hat{z}$ ,  $m_J = \frac{1}{2} \rightarrow m_J' = \frac{1}{2}$ , this becomes:

$$\mathcal{M}_{OR} = \frac{-e^3 B}{9} [\langle W \rangle + \langle V \rangle] \quad (53)$$

which yields the following numerical contribution to  $\mathcal{M}$

$$\mathcal{M}_{OR} = -1.20 \times 10^{-5} \mu_B \quad (54)$$



### 3.4 Total Theoretical M1 Rate;

#### Corrections to $g_J(Tl, 6^2P_{1/2})$

We collect the four contributions to the M1 amplitude (Eqs. (32), (43), (51) and (54):

$$\mathcal{M} = \mathcal{M}_{REL} + \mathcal{M}_{II} + \mathcal{M}_L + \mathcal{M}_{OR} = -3.2 \times 10^{-5} \mu_B \quad (55)$$

Our analysis of hyperfine structure indicates that the uncertainty of  $\sim 20\%$  in the calculation of relativistic  $\mathcal{M}_{REL}$  and  $\mathcal{M}_{OR}$ . In addition,  $\mathcal{M}_{II}$  has an independent uncertainty of  $\sim 15\%$ . The combined theoretical uncertainty of  $\mathcal{M}$  (Eq. 55) is estimated to be  $\sim 1.0 \times 10^{-5} \mu_B$ .

The Zeeman energy shift in a constant magnetic field B is related to  $g_J$  by:

$$\Delta E = \mu_B g_J m_J B \quad (56)$$

In zeroth order

$$g_J = \frac{J(J+1) + L(L+1) - S(S+1)}{2J(J+1)} + g_S \frac{J(J+1) + S(S+1) - L(L+1)}{2J(J+1)}$$

where  $g_S = 2.002319114$ . The corrections to  $g_J$  are obtained in the same manner as those described in Secs. 3.1 - 3.3, merely by computing  $6^2P_{1/2} - 6^2P_{1/2}$  diagonal matrix elements. The results of this calculation are displayed in Table 5 and compared with experiment.<sup>19</sup> The agreement is very good.

## 3.5 Hyperfine Mixing

Next, we calculate the additional contributions to the M1 amplitude arising from admixture to 6P, 7P wave-functions of 7P, 6P components, respectively, due to hyperfine interaction. According to first order perturbation theory,

$$|\overline{6^2P_{1/2}, F}\rangle = |6^2P_{1/2}, F\rangle + \frac{\langle 7^2P_{1/2}, F | H_{\text{HFS}} | 6^2P_{1/2}, F \rangle}{E_{6p} - E_{7p}} |7^2P_{1/2}, F\rangle \quad (57)$$

$$|\overline{7^2P_{1/2}, F'}\rangle = |7^2P_{1/2}, F'\rangle + \frac{\langle 6^2P_{1/2}, F' | H_{\text{HFS}} | 7^2P_{1/2}, F' \rangle}{E_{7p} - E_{6p}} |6^2P_{1/2}, F'\rangle \quad (58)$$

where the  $|\dots\rangle$  indicates a perturbed state, and  $H_{\text{HFS}}$ , given by Eq. (16), is diagonal in F, the total atomic angular momentum. This contributes to the M1 transition matrix element as follows:

$$\begin{aligned} \langle \overline{7^2P_{1/2}, F'} | M1 | \overline{6^2P_{1/2}, F} \rangle_{\text{HFS}} &\cong (\langle 7P, F | H_{\text{HFS}} | 6P, F \rangle - \langle 6P, F' | H_{\text{HFS}} | 7P, F' \rangle) \\ &\cdot \frac{1}{E_{6p} - E_{7p}} \cdot \langle nP_{1/2}, F' | M1 | nP_{1/2}, F \rangle \end{aligned} \quad (59)$$

where on the RHS we use the non-relativistic M1 operator, whose matrix elements are independent of principal quantum number n. It is interesting to note that the LHS of Eq. (59) vanishes for  $F = F'$ ; thus this correction, unlike the previous ones, only affects  $F = 0 \rightarrow F' = 1$  and  $F = 1 \rightarrow F' = 0$  transitions. The hyperfine matrix elements on the RHS may be computed by the methods of Sec. 2.3 with the following results:

For  $F = 0, F' = 1,$

$$\langle M1 \rangle_{\text{HFS}}^{F'=1, F=0} = +2.6 \times 10^{-6} \mu_B \quad (60)$$

For  $F = 1, F' = 0,$

$$\langle M1 \rangle_{\text{HFS}}^{F'=0, F=1} = -2.6 \times 10^{-6} \mu_B \cdot \sqrt{\frac{1}{3}} \quad (61)$$

### 3.6 Other M1 Transitions

The methods outlined in Secs. 3.1 - 3.3, 3.5 may be used to calculate other T& M1 transitions, forbidden or allowed. These include the  $6^2P_{1/2} - 6^2P_{3/2}$  transition (allowed) which has been suggested as an interesting candidate for a neutral current experiment, and the  $6^2P_{1/2} - 7^2P_{3/2}, 6^2P_{3/2} - 7^2P_{1/2}$  transitions which are not so strongly forbidden as  $nP_{1/2} - n'P_{1/2}$  and  $nP_{3/2} - n'P_{3/2}$  cases, since for  $1/2 \rightarrow 3/2$  or  $3/2 \rightarrow 1/2$  the radial wave functions are not fully orthogonal. In what follows we ignore the small higher-order effects considered in Secs. 3.2, 3.3, 3.5, and consider only the one-electron amplitude of Eq. (28). For  $nP_{3/2} - nP_{1/2}$  transitions we find

$$A_{3/2 \rightarrow 1/2} = 2\pi |\overline{V}_{fi}|^2 = e^2 \omega^3 \left| \int \frac{g_1(kr)}{\omega} (f_{3/2} g_{1/2} + g_{3/2} f_{1/2}) \right|^2 \quad (62)$$

and similarly for  $1/2 \rightarrow 3/2$  transitions. The results are tabulated in Table 6. In the allowed cases, the M1 matrix elements are within 2% of the non-relativistic value  $-\sqrt{2}/3$ , while the forbidden ( $6^2P_{1/2} - 7^2P_{3/2}, 6^2P_{3/2} - 7^2P_{1/2}$ ) matrix elements are about 10% of the allowed values, which corresponds to the expected magnitude of spin-orbit coupling effects.

These transitions also have non-zero electric quadrupole (E2) amplitudes. We obtain:

$$A_{E2} \cong \frac{1}{75} e^2 \omega^5 \left[ \int_0^\infty f_f r^2 f_i dr \right]^2 \quad (63)$$

since the portion of the E2 amplitude which is proportional to  $\int g_f r^2 g_i dr$  is quite negligible. Table 6 includes a tabulation of the E2 radial integrals and resulting A coefficients. The coefficient  $A_{E2} (6^2P_{3/2} \rightarrow 6^2P_{1/2})$  has also been calculated by Garstang<sup>20</sup> and his result (.11 sec<sup>-1</sup>) and ours are in agreement.

#### 4. PARITY VIOLATING E1 AMPLITUDES

##### 4.1 $6^2P_{1/2} \rightarrow 7^2P_{1/2}$ Transition

As previously discussed (Sec. 1) parity-violation in the electron-nucleon weak neutral interaction manifests itself in the matrix element:

$$\langle \psi_1 | H_{PV} | \psi_2 \rangle = \frac{-G Q_w}{2\sqrt{2}} \psi_1^* (\vec{x}) \gamma_5 \psi_2 (\vec{x}) \Big|_{\vec{x}=0} \quad (64)$$

We write the perturbed 6P, 7P states as:

$$| \overline{6P_{1/2}} \rangle = | 6P_{1/2} \rangle + \sum_n \frac{\langle nS_{1/2} | H_{PV} | 6P_{1/2} \rangle}{E_{6P} - E_{nS}} | nS_{1/2} \rangle \quad (65)$$

$$| \overline{7P_{1/2}} \rangle = | 7P_{1/2} \rangle + \sum_n \frac{\langle nS_{1/2} | H_{PV} | 7P_{1/2} \rangle}{E_{7P} - E_{nS}} | nS_{1/2} \rangle \quad (66)$$

From (64) we obtain:

$$\langle nS_{1/2} | H_{PV} | n'P_{1/2} \rangle = \frac{i}{4\pi} \frac{G}{2} \frac{Q_w}{\sqrt{2}} \frac{1}{r^2} \left[ f_{ns}(r) g_{n'p}(r) - f_{n'p}(r) g_{ns}(r) \right]_{r=0} \cdot \delta_{m_s m_p} \quad (67)$$

This expression is averaged over the nucleus assuming a constant proton- and neutron- density. As an alternative, one may assume a point-like nucleus, and evaluate  $\langle nS | H_{PV} | n'P \rangle$  at the nuclear radius; this increases the numerical value by 6%. The E1 matrix element is obtained by evaluating:

$$\begin{aligned} \langle \overline{7P}_{\frac{1}{2}} | E1 | \overline{6P}_{\frac{1}{2}} \rangle &= \sum_{nS} \frac{\langle 7P_{\frac{1}{2}} | E1 | nS \rangle \langle nS | H_{PV} | 6P_{\frac{1}{2}} \rangle}{E_{6P} - E_{nS}} \\ &+ \sum_{nS} \frac{\langle 7P_{\frac{1}{2}} | H_{PV} | nS \rangle \langle nS | E1 | 6P_{\frac{1}{2}} \rangle}{E_{7P} - E_{nS}} \end{aligned} \quad (68)$$

For the E1 matrix elements on RHS of Eq. (68) we have

$$\begin{aligned} \langle nS | E1 | P_{\frac{1}{2}} \rangle &= e \langle nS | \hat{\epsilon} \cdot r | P_{\frac{1}{2}} \rangle = e \int f_S r f_P dr \cdot \chi_{-1}^{m_S} \hat{\epsilon} \cdot \vec{e}_r \chi_1^{m_P} \\ &= \frac{e}{3} \int f_S r f_P dr, \quad (m_S = m_P = -\frac{1}{2}) \end{aligned} \quad (69)$$

Expression (68) is evaluated by two methods:

1. A sum is taken over the lowest five states  $|6s^2 ns\rangle$ ,  $n > 6$ ; and the effect of the autoionizing  $|6s 6p 7p\rangle$  state is also taken into account by including in the sum a term corresponding to the unphysical state  $|6s^2 6s\rangle$ . (See Appendix B for this argument.)

2. The operators  $\sum_n \frac{|nS\rangle \langle nS|}{E_{n'P} - E_{nS}}$  are replaced by Dirac Green's functions, described in detail in Appendix C. This calculation includes the contribution of all intermediate S-states including continuum and autoionizing states and is thus more reliable and complete than method 1.

The results are summarized in Table 7. The Green's function method yields the numerical value for  $\&_{PV} = \langle 7P_{\frac{1}{2}} | E1 | 6P_{\frac{1}{2}} \rangle$  in Eq. (68):

$$\&_{PV} = 1.93 i \cdot 10^{-10} Q_W |\mu_B| \quad (70)$$

which corresponds to an A coefficient:

$$A = 1.20 \cdot 10^{-16} Q_W^2 \text{ sec}^{-1} \quad (71)$$

In the Weinberg model,

$$Q_W = Z (1 - 4 \sin^2 \theta_W) - N \approx -140 \quad (72)$$

for Tl, using  $\sin^2 \theta_W = 0.3$  as suggested by the experiment of Reines et al.<sup>22</sup> Thus we obtain from (70) and (72):

$$\&_{PV} = -2.70 i \cdot 10^{-8} |\mu_B| \quad (73)$$

For the circular dichroism  $\delta$  it can be shown that one obtains:

$$\delta = \frac{2 \text{Im}(\&_{PV}) \mathcal{M}}{|\mathcal{M}|^2 + |\&|^2} \approx \frac{2 \text{Im}(\&_{PV})}{\mathcal{M}} \quad (74)$$

Inserting (73) and the experimental value of  $\mathcal{M}$  from Eq. (3) in 74 we obtain:

$$\delta = -2.6 \cdot 10^{-3} \quad (75)$$

This result is to be compared with the calculation of Sushkov, Flambaum, and Khriplovich,<sup>22</sup> who obtain, also using  $\mathcal{M}_{\text{expt}}$  from Eq. (3),

$$\delta = -2.5 \cdot 10^{-3} \quad (76)$$

To calculate  $\&_{PV}$ , they use non-relativistic hydrogenic wave-functions with an empirically determined correction factor. Their radial E1 integrals are extracted from experimental evidence where available, or from numerical calculations, and a finite sum over the five nearest levels is performed. It can be seen from Table VII that our complete Green's function evaluation differs from our finite sum by about 20%. The close agreement of Eqs. (75) and (76) is therefore somewhat fortuitous.

## 4.2 Other Parity-Violating Transitions

For  $P_{1/2} - P_{3/2}$  transitions we may ignore the effect of  $H_{PV}$  on the  $P_{3/2}$  state since  $J = 3/2$  wave functions have extremely small amplitudes at the nucleus. Thus,

$$\langle \overline{P_{3/2}} | E1 | \overline{P_{1/2}} \rangle = \sum_{nS} \frac{\langle P_{3/2} | E1 | nS \rangle \langle nS | H_{PV} | P_{1/2} \rangle}{E_{P_{1/2}} - E_{nS}} \quad (77)$$

These matrix elements were evaluated in the same way as described above for  $\mathcal{E}_{PV}$ . The results are summarized in Table 8, where

$$\langle P_{3/2} | E1 | nS \rangle = \frac{e\sqrt{2}}{3} \int_0^{\infty} f_{P_{3/2}} r f_{S_{1/2}} dr \quad (77a)$$

## 5. STARK EFFECT

### 5.1 $6^2P_{1/2} - 7^2P_{1/2}$ Transitions

We now calculate the electric-field-induced E1 transitions which can occur between  $6^2P_{1/2}$ ,  $7^2P_{1/2}$  levels through Stark-mixing with  $2^2S_{1/2}$ ,  $2^2D_{3/2}$  states. The coordinate system is shown in Fig. 2. Action of the perturbation  $H' = e\vec{E} \cdot \vec{r} = eE y$  results in the perturbed states:

$$\begin{aligned} |\overline{NP_{1/2}}\rangle &= |NP_{1/2}\rangle + \sum_{nS} \frac{|nS\rangle \langle nS | eE_0 y | NP_{1/2}\rangle}{E_{NP_{1/2}} - E_{nS}} \\ &+ \sum_{nD_{3/2}} \frac{|nD_{3/2}\rangle \langle nD_{3/2} | eE_0 y | NP_{1/2}\rangle}{E_{NP_{1/2}} - E_{nD_{3/2}}} \end{aligned} \quad (78)$$

Thus an electric dipole transition stimulated by laser photons with linear polarization

$$\hat{\epsilon} = \cos\theta \hat{y} + \sin\theta \hat{z} \quad (79)$$

has amplitude:

$$\begin{aligned} \epsilon_s &= \overline{\langle 7^2 P_{1/2} | E_1 | 6^2 P_{1/2} \rangle} \text{Stark} = \\ n = S_{1/2}, D_{3/2} \text{ states} & \left\{ \begin{aligned} & \sum_n \frac{\langle 7^2 P_{1/2} | e\hat{\epsilon} \cdot \vec{r} | n \rangle \langle n | eE_0 y | 6^2 P_{1/2} \rangle}{E_{6P_{1/2}} - E_n} + \\ & \sum_n \frac{\langle 7^2 P_{1/2} | eE_0 y | n \rangle \langle n | e\hat{\epsilon} \cdot \vec{r} | 6^2 P_{1/2} \rangle}{E_{7P_{1/2}} - E_n} \end{aligned} \right. \quad (80) \end{aligned}$$

The result of a calculation of this amplitude may be represented by a 2x2 matrix whose rows and columns are labelled by  $m_J(6^2 P_{1/2})$  and  $m_J(7^2 P_{1/2})$  respectively:

$$\begin{aligned} \epsilon_s &= e^2 E_0 \cdot \\ & \quad \begin{array}{cc} & \begin{array}{c} \frac{1}{2} \\ -\frac{1}{2} \end{array} \\ \begin{array}{c} \frac{1}{2} \\ -\frac{1}{2} \end{array} & \begin{array}{cc} & -\frac{1}{2} = m_J(6^2 P_{1/2}) \\ \hline m_J(7^2 P_{1/2}) = \frac{1}{2} & \begin{array}{cc} \alpha \cos \theta & -i\beta \sin \theta \\ -i\beta \sin \theta & \alpha \cos \theta \end{array} \end{array} \end{array} \quad (81) \end{aligned}$$

Here

$$\begin{aligned} \alpha &= \frac{1}{9} \sum_{nS} R_{7P,nS} R_{6P,nS} \left( \frac{1}{E_7 - E_{nS}} + \frac{1}{E_6 - E_{nS}} \right) \\ &+ \frac{2}{9} \sum_{nD_{3/2}} R_{7P,nD} R_{6P,nD} \left( \frac{1}{E_7 - E_{nD}} + \frac{1}{E_6 - E_{nD}} \right) \quad (82) \end{aligned}$$

and

$$\begin{aligned} \beta &= \frac{1}{9} \sum_{nS} R_{7P,nS} R_{6P,nS} \left( \frac{1}{E_6 - E_{nS}} - \frac{1}{E_7 - E_{nS}} \right) \\ &+ \frac{1}{9} \sum_{nD_{3/2}} R_{7P,nD} R_{6P,nD} \left( \frac{1}{E_7 - E_{nD}} - \frac{1}{E_6 - E_{nD}} \right) \quad (83) \end{aligned}$$



where  $E_6 = E(6^2P_{1/2})$ ,  $E_7 = E(7^2P_{1/2})$ , and  $R_{7P,nS} = \langle 7^2P_{1/2} | r | n^2S_{1/2} \rangle$ , etc.

The quantities  $\alpha$  and  $\beta$  have been evaluated by summing over the nearest S and D states, and also by use of the Green's function, Appendix C.

The results are summarized in Table 9.

Chu, Commins and Conti have measured  $\beta/\alpha$ . Their result:<sup>3</sup>

$$\beta/\alpha]_{\text{expt}} = 0.84 \quad (84)$$

is in good agreement with the Green's function value of Table 9. This theoretical value  $\beta/\alpha = 0.80$  was employed by them to determine the experimental value of  $\mathcal{M}$ , as described below.

### 5.2 Experimental Determination of M1 Amplitude

A finite  $7^2P_{1/2}$  final state polarization can arise along the  $\hat{z}$  axis of Fig. 5.1 through interference between  $\mathcal{M}$  and/or  $\mathcal{E}_{PV}$  and  $\mathcal{E}_S$ . Interference between  $\mathcal{M}$  and  $\mathcal{E}_S$  may then be utilized to measure  $\mathcal{M}$ . Here the effects of  $\mathcal{E}_{PV}$ , which are in any case very small, are neglected. In an extension of this experiment now underway, interference between  $\mathcal{E}_{PV}$  and  $\mathcal{E}_S$  is utilized to determine  $\mathcal{E}_{PV}$  itself.

In order to facilitate comparison with observations in which some of the hfs components of the  $6^2P_{1/2} - 7^2P_{1/2}$  transition are resolved, we replace the matrix of Eq. (81) by one whose rows and columns are labelled by  $F', m_{F'}$  (for  $7^2P_{1/2}$ ) and  $F, m_F$  (for  $6^2P_{1/2}$ ), respectively. Including  $\mathcal{E}_{PV}$ ,  $\mathcal{M}$  and  $\mathcal{E}_S$ , the total dipole amplitude  $D$  is given in Table 10.

In the experimental determination of  $\mathcal{M}$ , the  $6^2P_{1/2}$  hfs splitting, but not that of  $7^2P_{1/2}$ , is resolved. Thus the  $7^2P_{1/2}$  polarization is given by the formula:

$$P(F) = \frac{\sum_{m_F, m_{F'}}^{m_{F'}} |D_{F, m_F}^{F', m_{F'}}|^2}{\sum_{m_F, m_{F'}} |D_{F, m_F}^{F', m_{F'}}|^2} \quad (85)$$

Neglecting  $|\mathcal{M}|^2$  compared to  $|\mathcal{E}_S|^2$  (which is justifiable for the rather large E fields employed) Eq. (84) becomes the following for the four indicated cases of interest:

a)	$F = 1, F' = 1$	$\hat{\epsilon} \parallel \vec{E} (\Theta=0)$	$P \approx \frac{4}{3} \frac{\mathcal{M}}{\alpha}$
b)	$F = 0; F' = 0$	$\hat{\epsilon} \parallel \vec{E} (\Theta=0)$	$P = 0$
c)	$F = 1; F' = 1, 0$	$\hat{\epsilon} \perp \vec{E} (\Theta=90^\circ)$	$P = -\frac{2}{3} \frac{\mathcal{M}}{\beta} (7^2 P_{\frac{1}{2}} \text{ hfs unresolved})$
d)	$F = 0; F' = 1$	$\hat{\epsilon} \perp \vec{E} (\Theta=90^\circ)$	$P = -2 \frac{\mathcal{M}}{\beta}$

We now apply the hfs mixing correction of Eq. (60) to case d) (it also applies to case c but this was not observed in detail). The resulting ratio  $P_d^{\text{corr.}}/P_a$  is then in good agreement with experiment. From their measurements of  $P_a$  and/or  $P_d$  Chu et al<sup>3</sup> obtain the experimental value of  $\mathcal{M}$  given in Eq. (3).

### 5.3 Interference of $\mathcal{E}_{PV}$ and $\mathcal{E}_S$

When the incident light is circularly polarized, it becomes possible to measure the interference between  $\mathcal{E}_{PV}$  and  $\mathcal{E}_S$ , again by detecting the polarization of the  $7^2P_{\frac{1}{2}}$  state (by means of circular polarization of its decay fluorescence). The formulae analogous to Eq. (85) are readily obtained from Table 10. We quote only the result for the  $F = 0 \rightarrow F' = 1$  transition:

$$P = \frac{\frac{1}{2}(\beta-f)^2 - \frac{1}{2}(\beta+f)^2}{\frac{1}{2}(\beta+f)^2 + \frac{1}{2}(\beta-f)^2 + f^2} \approx \frac{-2f}{\beta} \quad (86)$$

where  $f = \mathcal{M} - \eta \mathcal{E}_{PV}$ ,  $\eta = \pm 1$  for RHC (LHC) laser light, and the approximation  $P \approx \frac{-2f}{\beta}$  is valid for large electric fields ( $E \gg 1$  V/cm).

#### 6. PARITY VIOLATION IN ${}^2P_{1/2} - {}^2P_{3/2}$ TRANSITIONS

For the transitions  $6^2P_{1/2} - 6^2P_{3/2}$ ,  $6^2P_{1/2} - 7^2P_{3/2}$ , and  $6^2P_{3/2} - 7^2P_{1/2}$ , we include E2 as well as M1 contributions and write:

$$\langle T \rangle = \langle P_{3/2} | \vec{\mu} \cdot \vec{\mathcal{X}} \times \vec{\mathcal{E}} + e \hat{\mathcal{E}} \cdot \vec{r} + i e (\hat{\mathcal{E}} \cdot \vec{r}) (\vec{k} \cdot \vec{r}) | P_{1/2} \rangle \quad (87)$$

where  $\vec{\mu} = \frac{e\hbar}{2mc} (\vec{L} + \vec{S})$ , and  $\hat{\mathcal{E}} = \hat{y} \cos\theta + \hat{z} \sin\theta$ .

The resulting transition matrix is given in Table 11. The polarization is calculated as in Eq. (86) with the result

$$P = \frac{2\mathcal{M} \cdot \text{Im}(\mathcal{E}_{PV})}{|\mathcal{M}|^2 + \frac{2}{3} |\langle \mathcal{E}_2 \rangle|^2} \quad (88)$$

The numerical results are summarized in Table 12.

The transition  $6^2P_{1/2} - 6^2P_{3/2}$  has been discussed as a candidate for optical rotation experiments to detect parity violation. We compare our value of the  $6^2P_{1/2} - 6^2P_{3/2}$  polarization  $4.17 \cdot 10^{-7}$ , with that obtained from the calculation of Henley and Wilets:<sup>23</sup>

$$P = 4.80 \cdot 10^{-7}, \text{ for } \sin^2\theta_w = 0.3 \quad (89)$$

The discrepancy of 15% is largely due to the  $\langle \mathcal{E}_2 \rangle$  amplitude which Henley & Wilets ignored. Once this correction is made, the two calculations agree within 2%.

Henley and Wilets used a Green's function technique with hybrid Dirac-Schroedinger wave functions; that is, relativistic wave functions are calculated for very small  $r$  and matched to non-relativistic functions at larger  $r$ . Empirical energies rather than calculated energies (which in their case differ by  $\sim 20\%$ ) are inserted, although it is claimed that this does not change  $\epsilon_{PV}$  substantially. Since Henley and Wilets do not report calculations of  $T\ell$  parameters other than  $\epsilon_{PV}$  ( $6^2P_{1/2}-6^2P_{3/2}$ ) we cannot make an accurate comparison of their calculation with ours or with experiments.

We note in passing that in calculations<sup>23,24</sup> of the optical rotation of the currently investigated  $4S_{3/2}-2D_{3/2}$  and  $4S_{3/2}-2D_{5/2}$  transitions in bismuth, the effect of  $\langle \epsilon_2 \rangle$  is ignored. In the calculations of Garstang<sup>20</sup> for these transitions, the  $\epsilon_2$  amplitude in  $4S_{3/2}-2D_{3/2}$  is in fact negligible, but the large  $\epsilon_2$  amplitude calculated for  $4S_{3/2}-2D_{5/2}$  would reduce the optical rotation by  $\sim 30\%$ . A more precise calculation may alter this result substantially.

The  $T\ell$  transitions  $6^2P_{3/2}-7^2P_{1/2}$ ,  $6^2P_{1/2}-7^2P_{3/2}$  may also be considered in optical rotation experiments, although the experimental difficulties are formidable.

ACKNOWLEDGEMENTS

We thank Professor C. Schwartz, Dr. Peter Mohr, and Dr. Steven Chu for numerous useful discussions.

## REFERENCES

1. F.J. Hasert et al., Phys. Lett. 46B, 121, 138 (1973), Nucl. Phys. B73, 1 (1974).  
A. Benvenuti et al., Phys. Rev. Lett. 32, 800 (1974), Phys. Rev. Lett. 37, 1039 (1976).  
B. Aubert et al., Phys. Rev. Lett. 32, 1454 (1974).  
S.J. Barish et al., Phys. Rev. Lett. 33, 418 (1974), Phys. Rev. Lett. 36, 179 (1976).  
B.C. Barish et al., Phys. Rev. Lett. 34, 538 (1975).  
W. Lee et al., Phys. Rev. Lett. 37, 186 (1976).  
see Albright, C.H. et al., FERMILAB-Pub.-76/40-Thy preprint for a recent review of the high energy experimental situation.
2. S. Weinberg, Phys. Rev. Lett. 19, 1264 (1967), Phys. Rev. Lett. 27, 1688 (1971), Phys. Rev. D5, 1412 (1972).  
A. Salam, in Elementary Particle Theory ed. N. Svartholm (Stockholm: Almqvist and Forlag) 1968.  
For a review of renormalizable gauge theories, see T.D. Lee, Phys. Rep. 9C, no. 2 (1974) and J.C. Taylor, Gauge Theories of Weak Interactions, Cambridge University Press (1976).
3. S. Chu, R. Conti and E.D. Commins, Phys. Lett. A 60A, 96 (1977).  
S. Chu, Ph.D. thesis, Lawrence Berkeley Laboratory preprint LBL - 5731.

4. M.A. Bouchiat and C.C. Bouchiat, Phys. Lett. 48B, 111 (1974),  
Jour. de Phys. 35, 899 (1974), Jour. de Phys. 36, 493 (1975).
5. T. Tietz, J. Chem. Phys. 22, 2094 (1954).
6. M.E. Rose, Relativistic Electron Theory, J. Wiley & Sons, Inc.,  
New York (1961). Our f and g are not the same as Rose's.
7. C. Schwartz, Phys. Rev. 97, 380 (1955), Phys. Rev. 105, 173 (1957).
8. M. Abramowitz and I.A. Stegun, Handbook of Mathematical Functions,  
AMS 55, Nat. B. of Stand. (1964).
9. C.M. Lederer, J.M. Hollander, and I. Perlman, Table of Isotopes,
10. V.B. Berestetskii, E.M. Lifshitz, L.P. Pitaevskii, Relativistic  
Quantum Theory, (Vol. 4, pt. I of Course of Theoretical  
Physics) Pergamon Press, London (1971).
11. A. Gallagher and A. Lurio, Phys. Rev. 136, A87 (1964).
12. E.M. Anderson, E.K. Anderson and V.F. Trusov, Opt. i Spekt. 22,  
471 (861) (1967).
13. W.R. Johnson, Phys. Rev. Lett. 29, 1123 (1972).
14. M. Phillips, Phys. Rev. 88, 209 (1952).
15. G. Breit, Phys. Rev. 34, 553 (1929), Phys. Rev. 39, 616 (1932).
16. A. Abragam and J.H. Van Vleck, Phys. Rev. 92, 1448 (1953).
17. C. Schwartz, unpublished communication (1970).
18. W.E. Lamb, Jr., Phys. Rev. 60, 817 (1941).
19. T.R. Fowler, Ph.D. thesis (UCRL-18321), University of California,  
Berkeley (1968).
20. R.H. Garstang, J. of Research NBS-A 68, 61 (1964).

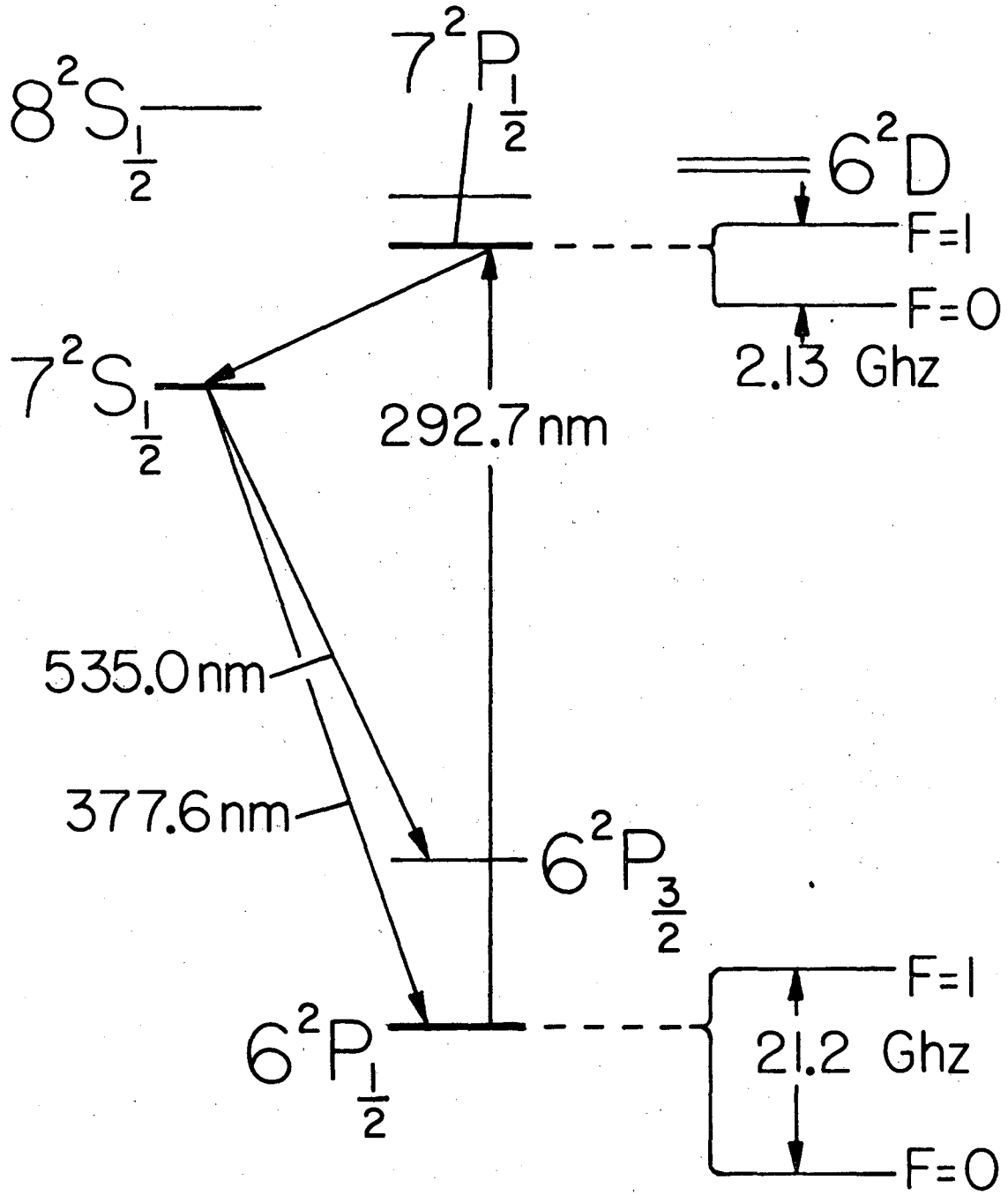
21. F. Reines et al., Phys. Rev. Lett. 37, 315 (1976).
22. O.P. Sushkov, V.V. Flambaum, and I.B. Khriplovich, JEPT Lett. 24, 502 (1976).
23. E.M. Henley and L. Wilets, Phys. Rev. A 14, 1411 (1976).
24. M. Brimicombe, C.E. Loving, and P.G.H. Sanders, J. Phys. B. Atom. Molec. Phys. 9, L237 (1976).
25. E. Fermi and E. Segre, Zeit. Phys. 82, 729 (1933).
26. G.F. Koster, Phys. Rev. 86, 148 (1952).
27. P.J. Mohr, Ann. of Phys. 88, 26 (1974).
28. M. Gyulassy, Nucl. Phys. A, A244, 497 (1975).



FIGURE CAPTIONS

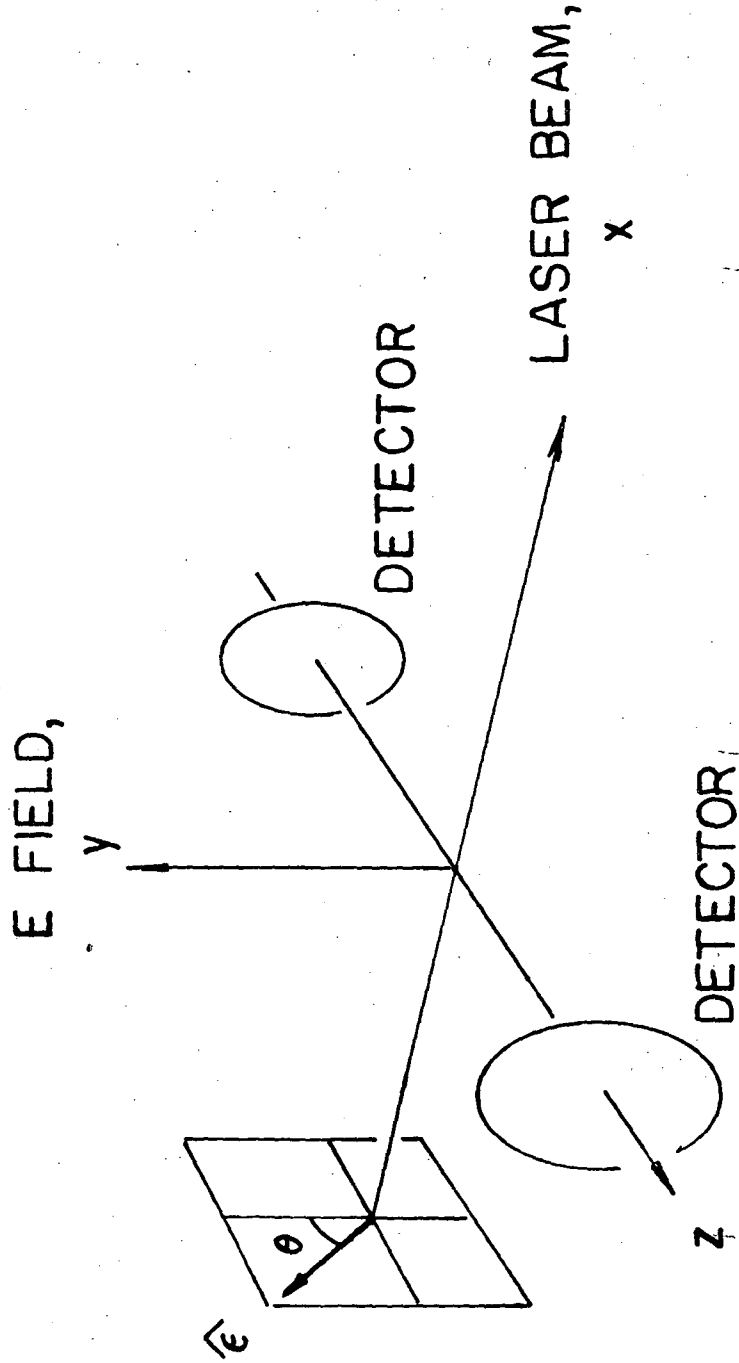
Figure 1 Low-lying energy levels of the Tl atom (not to scale). The hyperfine structure splittings of  $6^2P_{1/2}$ ,  $7^2P_{1/2}$  states are shown. Absorption of the  $6^2P_{1/2}$ - $7^2P_{1/2}$  M1 photon (292.7 nm) is detected by observing fluorescence at 535 nm. accompanying decay of the  $7^2P_{1/2}$  state.

Figure 2 Coordinate system and orientation of electric field  $\vec{E}$ , laser beam, and detectors as described in this paper and utilized in the experiment of Chu, Commins and Conti.



XBL 773-7971

Fig. 1



XBL 773-7970

Fig. 2

## APPENDIX A

Interconfiguration Interaction and Hyperfine Structure  
of the  $6^2P_{3/2}$  State

It is well known that the observed hfs of the  $6^2P_{3/2}$  state in Tl differs markedly from that calculated in the OEFC approximation using the single  $5d^{10} 6s^2 6p_{3/2}$  configuration, because the actual atomic state contains admixtures of other configurations,<sup>2</sup> notably (...6s 7s 6p). We write the unperturbed wave function (...6s<sup>2</sup>6<sub>p</sub>) as  $\psi_0$  and form two possible  $P_{3/2}$  (or  $P_{1/2}$ ) states from the 6s 7s 6p configuration. These are  $\psi_1$  (6s 7s (<sup>3</sup>S<sub>1</sub>) 6p <sup>2</sup>P<sub>J</sub>) with the 2 s electrons in a spin-one state, and  $\psi_2$  (6s 7s (<sup>1</sup>S<sub>0</sub>) 6p <sup>2</sup>P<sub>J</sub>) with the total s electron spin equal to zero. The states and notation are similar to those of Koster,<sup>2</sup> who performs a similar calculation for gallium. We write for the total wave-function:

$$\psi = \alpha_0 \psi_0 + \alpha_1 \psi_1 + \alpha_2 \psi_2 \quad (\text{A1})$$

The coefficients  $\alpha_1, \alpha_2$  are given in first order perturbation theory by

$$\alpha_1 = \frac{\langle \psi_1 | V | \psi_0 \rangle}{E_0 - E_1} \quad (\text{A2})$$

and

$$\alpha_2 = \frac{\langle \psi_2 | V | \psi_0 \rangle}{E_0 - E_2} \quad (\text{A3})$$

where  $V = \sum_{i < j} \frac{e^2}{r_{ij}}$  and the matrix elements of V in A2, A3 are calculated from the electrostatic integral:

$$F_0(6s, 6s; 6s, 7s) = \iint \psi_{6s}(\vec{x}_1) \psi_{6s}(\vec{x}_2) \frac{e^2}{r_{12}} \psi_{6s}(\vec{x}_1) \psi_{7s}(\vec{x}_2) d\tau_1 d\tau_2$$

and the similar and direct exchange integrals  $F_0(6s, 6p; 7s, 6p)$  and  $G_1(6s, 6p; 6p, 7s)$ . We use the 6s wave-function (ionization energy =  $2.3376 \cdot 10^{-5}$ ) calculated from Eq. (4). This is not self-consistent, since that central potential already includes the  $6s^2$  charge distribution. However, this introduces an error estimated at only 10 to 15% in the ionization energy. The 7s and  $6p_J$  states are calculated in the same central potential, and the energy denominator is approximated by the 6S-7S energy difference. Normalizing with  $\alpha_0^2 + \alpha_1^2 + \alpha_2^2 = 1$ , we find:

$$\begin{aligned} 6P_{1/2}: \quad \alpha_0 &= .97 \quad \alpha_1 = +.0097 \quad \alpha_2 = +.23 \\ 6P_{3/2}: \quad \alpha_0 &= .97 \quad \alpha_1 = .029 \quad \alpha_2 = .22 \end{aligned} \tag{A4}$$

The large difference  $\alpha_1(P_{3/2}) - \alpha_1(P_{1/2})$  occurs because of a corresponding difference in the exchange integral  $G_1(6s, 6p; 6p, 7s)$  between  $6P_{3/2}$  and  $6P_{1/2}$  states.

The hfs splitting is:

$$\begin{aligned} \Delta_{3/2} &= \Delta_0(6^2P_{3/2}) + \frac{4}{9} \alpha_1^2 (\Delta_{6s} + \Delta_{7s}) \\ &\quad - \frac{4}{3\sqrt{3}} \alpha_1 \alpha_2 (\Delta_{6s} - \Delta_{7s}) - \frac{2}{3\sqrt{6}} \alpha_1 \alpha_2 \sqrt{\Delta_{6s} \Delta_{7s}} \\ \Delta_{1/2} &= \Delta_0(6^2P_{1/2}) + \frac{2}{9} \alpha_1^2 (\Delta_{6s} + \Delta_{7s}) + \frac{2}{3\sqrt{3}} \alpha_1 \alpha_2 (\Delta_{6s} - \Delta_{7s}) \\ &\quad + \frac{4}{3\sqrt{6}} \sqrt{\Delta_{6s} \Delta_{7s}} \end{aligned} \tag{A5}$$

where only the dominating s-electron perturbation is included.

In formulae (A5) we use the experimental value of  $\Delta_{7S}$ , Eq. (A4), and the calculated value  $\Delta_{6S} = 135$  Ghz. The numerical results are summarized in Table A1. They show that the  $6^2P_{3/2}$  hfs is strongly affected by configuration mixing while the  $6^2P_{1/2}$  hfs is not. Further, similar corrections can be obtained for  $6sns6p$  configurations with  $n > 7$ . That of the  $6s8s6p$  and  $6s9s6p$  configurations is also included in Table A1. We find for  $6s8s6p_{3/2}$ :  $\alpha_1 = .012$ ,  $\alpha_2 = .09$ ; while for  $6s9s6p_{3/2}$ ,  $\alpha_1 = .007$ ,  $\alpha_2 = .05$ .

Because of the uncertainties and lack of self-consistency inherent in the present approach, there is no profit in attempting to include contributions of configurations  $6sns6p_{3/2}$  with  $n > 9$ .

Table AI.

State	Unperturbed Hfs splitting: $\Delta E_0$	Hfs splitting including (6s7s6p) correction: $\Delta E_1 = \Delta E_0 + \delta(6s7s6p)$	$\Delta E_2 = \Delta E_1 + \delta(6s8s6p) + \delta(6s9s6p)$	Observed Hfs splitting
$6^2P_{1/2}$	21.8 Ghz	22.1	22.1	21.33
$6^2P_{3/2}$	3.27 Ghz	1.37	.81	.518

## APPENDIX B

We demonstrate that the effect of the  $6s6p7p$  autoionizing state is taken into account (approximately) by calculating the amplitude  $\mathcal{E}_{PV}$  if a term corresponding to the unphysical  $6s^2 6s$  state is included. The term in question is:

$$T = \frac{\langle 6s6s7p | \hat{\epsilon} \cdot \mathbf{r} | 6s6p7p \rangle \langle 6s6p7p | H'_{PV} | 6s6s6p \rangle}{E_{6s6s6p} - E_{6s6p7p}} + \frac{\langle 6s6s7p | H'_{PV} | 6s6p7p \rangle \langle 6s6p7p | \hat{\epsilon} \cdot \mathbf{r} | 6s6s6p \rangle}{E_{6s6s7p} - E_{6s6p7p}} \quad (B1)$$

Now:

$$\begin{aligned} \langle 6s6s7p | \hat{\epsilon} \cdot \vec{r} | 6s6p7p \rangle \langle 6s6p7p | H' | 6s6s6p \rangle &= \\ - \langle 6s | \hat{\epsilon} \cdot \vec{r} | 6p \rangle \langle 7p | H'_{PV} | 6s \rangle &= \\ - \langle 7p | H'_{PV} | 6s \rangle \langle 6s | \hat{\epsilon} \cdot \vec{r} | 6p \rangle, & \end{aligned} \quad (B2)$$

and

$$\begin{aligned} \langle 6s6s7p | H'_{PV} | 6s6p7p \rangle \langle 6s6p7p | \hat{\epsilon} \cdot \vec{r} | 6s6s6p \rangle &= \\ - \langle 7p | \hat{\epsilon} \cdot \vec{r} | 6s \rangle \langle 6s | H'_{PV} | 6p \rangle & \end{aligned} \quad (B3)$$

$$\text{Furthermore } E_{6s6s7p} - E_{6s6p7p} \cong -(E_{6p} - E_{6s}) \quad (B4)$$

$$\text{and } E_{6s6s6p} - E_{6s6p7p} \cong -(E_{7p} - E_{6s}) \quad (B5)$$

Inserting B2 - B5 in B1 we obtain:

$$T = \frac{\langle 7p | \hat{\epsilon} \cdot \vec{r} | 6s \rangle \langle 6s | H'_{PV} | 6p \rangle}{E_{6p} - E_{6s}} + \frac{\langle 7p | H'_{PV} | 6s \rangle \langle 6s | \hat{\epsilon} \cdot \vec{r} | 6p \rangle}{E_7 - E_{6s}} \quad (B6)$$

which is the desired result.



APPENDIX C

Construction and Use of the Dirac Green's Function

The construction of the Dirac Green's function has been described by Mohr, and Gyulassy, with emphasis on the case of a spherically symmetric central potential. This function is a solution of the differential equation:

$$(H(\vec{r}_2) - E) G(\vec{r}_1, \vec{r}_2, E) = I \delta^3(\vec{r}_2 - \vec{r}_1) \quad (C1)$$

where H is the Dirac Hamiltonian with potential  $V(\vec{r}_2) = V(|\vec{r}_2|)$  and I is the 4x4 identity matrix. Separation of radial and angular variables is accomplished by writing

$$G(\vec{r}_2, \vec{r}_1, E) = \sum_{\kappa, \mu} \begin{pmatrix} G_{\kappa}^{11}(r_2, r_1, E) \chi_{\kappa}^{\mu}(\vec{e}_2) \chi_{\kappa}^{\mu \dagger}(\vec{e}_1) & -iG_{\kappa}^{12}(r_2, r_1, E) \chi_{\kappa}^{\mu}(\vec{e}_2) \chi_{-\kappa}^{\mu \dagger}(\vec{e}_1) \\ iG_{\kappa}^{21}(r_2, r_1, E) \chi_{-\kappa}^{\mu}(\vec{e}_2) \chi_{\kappa}^{\mu \dagger}(\vec{e}_1) & G_{\kappa}^{22}(r_2, r_1, E) \chi_{-\kappa}^{\mu}(\vec{e}_2) \chi_{-\kappa}^{\mu \dagger}(\vec{e}_1) \end{pmatrix} \quad (C2)$$

where the  $\chi_{\kappa}(\vec{e})$  are the same functions as defined in Eq. (13). Eq. (C2)

is justified by the completeness relation:

$$\sum_{\kappa, \mu} \chi_{\kappa}^{\mu}(\vec{e}_2) \chi_{\kappa}^{\mu \dagger}(\vec{e}_1) = \begin{pmatrix} 1 & 0 \\ 0 & 1 \end{pmatrix} \delta(\phi_2 - \phi_1) \delta(\cos\theta_2 - \cos\theta_1)$$

Only  $G_{\kappa=-1}^{ij}$  contributes to  $\mathcal{E}_{PV}$  ( $S_{1/2}$ -states) while for  $\mathcal{E}_S$  (Stark mixing), the terms  $G_{\kappa=-1}^{ij}$  ( $S_{1/2}$  states) and  $G_{\kappa=2}^{ij}$  ( $D_{3/2}$  states) contribute. Eq. (C1) reduces to a 2x2 radial equation:

$$\begin{pmatrix} 1+V(r_2)-E & -\frac{1}{r_2} \frac{\partial}{\partial r_2} (r_2) + \frac{\kappa}{r_2} \\ \frac{1}{r_2} \frac{\partial}{\partial r_2} (r_2) + \frac{\kappa}{r_2} & -1+V(r_2)-E \end{pmatrix} \begin{pmatrix} G_{\kappa}^{11}(r_2, r_1, E) & G_{\kappa}^{12}(r_2, r_1, E) \\ G_{\kappa}^{21}(r_2, r_1, E) & G_{\kappa}^{22}(r_2, r_1, E) \end{pmatrix} \\
 = \begin{pmatrix} 1 & 0 \\ 0 & 1 \end{pmatrix} \frac{\delta(r_2 - r_1)}{r_2 r_1} \quad (C3)$$

It can be shown that the solution of C3 is:

$$\begin{aligned}
 G_{\kappa}(r_2, r_1, E) &= \frac{1}{J^{\kappa}(E)} \left\{ \theta(r_2 - r_1) \begin{pmatrix} F_{<}^{\kappa}(r_2) F_{>}^{\kappa}(r_1) & F_{<}^{\kappa}(r_2) G_{>}^{\kappa}(r_1) \\ G_{<}^{\kappa}(r_2) F_{>}^{\kappa}(r_1) & G_{<}^{\kappa}(r_2) G_{>}^{\kappa}(r_1) \end{pmatrix} \right. \\
 &\quad \left. + \theta(r_1 - r_2) \begin{pmatrix} F_{>}^{\kappa}(r_2) F_{<}^{\kappa}(r_1) & F_{>}^{\kappa}(r_2) G_{<}^{\kappa}(r_1) \\ G_{>}^{\kappa}(r_2) F_{<}^{\kappa}(r_1) & G_{>}^{\kappa}(r_2) G_{<}^{\kappa}(r_1) \end{pmatrix} \right\} \quad (C4)
 \end{aligned}$$

where  $J^{\kappa}(E)$  is the Wronskian:

$$J^{\kappa}(E) = r^2 \left\{ G_{<}^{\kappa}(r) F_{>}^{\kappa}(r) - G_{>}^{\kappa}(r) F_{<}^{\kappa}(r) \right\}$$

and  $F^{\kappa}$ ,  $G^{\kappa}$  are solutions of the equation:

$$\begin{pmatrix} 1+V(r)-E & \left(-\frac{1}{r} \frac{d(r)}{dr} + \frac{\kappa}{r}\right) \\ \left(\frac{1}{r} \frac{d(r)}{dr} + \frac{\kappa}{r}\right) & -1+V(r)-E \end{pmatrix} \begin{pmatrix} F \\ G \end{pmatrix} = 0 \quad (C5)$$

$\begin{pmatrix} F_{<} \\ G_{<} \end{pmatrix}$  is the solution which is regular as  $r \rightarrow 0$ , while  $\begin{pmatrix} F_{>} \\ G_{>} \end{pmatrix}$  is the solution

regular as  $r \rightarrow \infty$ . These solutions are calculated in the same manner as the

eigenolutions of Eq. (11), that is, by numerical integration of the differential equation starting with the asymptotic solution either for small  $r$  (for  $F_<, G_<$  and using  $V(r)$  in (c) of Section 2.1 or for large  $r$  (for  $F_>, G_>$ , using  $V(r) \rightarrow \frac{-e^2}{r}$ ). We note that  $F, G$  of C5 correspond to  $f/r, g/r$  of Eq. (13).

The parity violating amplitude  $\mathcal{E}_{PV}$  of Eq. (68) can be written as:

$$\begin{aligned} \mathcal{E}_{PV} = & - \iint \langle \psi_{7\frac{1}{2}P_{\frac{1}{2}}}^{\mu_1}(\vec{r}_1) | e\vec{\epsilon} \cdot \vec{r} G(\vec{r}_1, \vec{r}_2, E_{6p}) H_{PV} | \psi_{6\frac{1}{2}P_{\frac{1}{2}}}^{\mu_2}(\vec{r}_2) \rangle d^3\vec{r}_2 d^3\vec{r}_1 \\ & - \iint \langle \psi_{7\frac{1}{2}P_{\frac{1}{2}}}^{\mu_1}(\vec{r}_1) | H_{PV} G(\vec{r}_1, \vec{r}_2, E_{7p}) e\vec{\epsilon} \cdot \vec{r} | \psi_{6\frac{1}{2}P_{\frac{1}{2}}}^{\mu_2}(\vec{r}_2) \rangle d^3\vec{r}_2 d^3\vec{r}_1 \end{aligned} \quad (C6)$$

Because of the short range character of  $H_{PV}$  the first term in C6 becomes:

$$\begin{aligned} & -e \int_0^\infty f_{7p}(r_2) r_2 F^{(\kappa=-1)}(r_2, E_6) dr_2 \cdot \int \chi_1^{m_1 \dagger} \vec{\epsilon} \cdot \vec{e}_r \chi_1^{m_2} \\ & \frac{iG_W}{8\pi\sqrt{2}} \cdot \frac{1}{J(E_6)R^2} \cdot \left\{ (RF_<^{(\kappa=-1)}(R, E_6) g_{6p}(R) - (RG_<^{(\kappa=-1)}(R, E_6)) f_{6p}(R)) \right\} \\ & \hspace{20em} R < r_{nuc} \end{aligned} \quad (C7)$$

In practice this expression is averaged over the region  $R \leq r_{nuc}$ , where  $r_{nuc}$  is the nuclear radius. The second term in C6 becomes:

$$\begin{aligned} & +e \int f_{6p}(r_1) r_1 F^{(\kappa=-1)}(r_1, E_7) dr_1 \cdot \int \chi_1^{m_1 \dagger} \vec{\epsilon} \cdot \vec{e}_r \chi_1^{m_2} \\ & \frac{iG_W}{8\pi\sqrt{2}} J(E_7)R^2 \left\{ (RF_<^{(\kappa=-1)}(R, E_7) g_{7p}(R) - (RG_<^{(\kappa=-1)}(R, E_7)) f_7(R) \right\} \end{aligned} \quad (C8)$$

A similar calculation was performed for  $\epsilon_S$  (Sec. 5). In this case only "large" components (f,F) contribute significantly. For example, the matrix element  $\alpha$  of Eq. (82) is written:

$$\alpha = -\frac{1}{9} \left[ \frac{\int_0^\infty \int_0^\infty f_{7p}(r_2) r_2 (r_{<} F_{<}^{(\kappa=-1)}(r_{<}, E_6)) (r_{>} F_{>}^{(\kappa=-1)}(r_{>}, E_6)) r_1 f_{6p}(r_1) dr_1 dr_2}{J(E_6)} + \frac{\int_0^\infty \int_0^\infty f_{7p}(r_2) r_2 (r_{<} F_{<}^{(\kappa=-1)}(r_{<}, E_7)) (r_{>} F_{>}^{(\kappa=-1)}(r_{>}, E_7)) r_1 f_{6p}(r_1) dr_1 dr_2}{J(E_7)} \right] - \frac{2}{9} \cdot \left[ \text{same as above with } \kappa = +2 \right] \quad (C9)$$

In all of the above expressions,

$r_{>} =$  larger of  $r_1, r_2$

$r_{<} =$  smaller of  $r_1, r_2$ .

The expression for  $\beta$  (Eq. 83) is obtained in the same way.

Table I. Dirac radial functions  $f/r$ ,  $g/r$  for selected states.

$r$ (*)	$6p_{1/2}$		$6p_{3/2}$		$7p_{1/2}$		$7s_{1/2}$		$6d_{3/2}$	
	$\frac{f(r)}{r}$	$\frac{g(r)}{r}$	$\frac{f(r)}{r}$	$\frac{g(r)}{r}$	$\frac{f(r)}{r}$	$\frac{g(r)}{r}$	$\frac{f(r)}{r}$	$\frac{g(r)}{r}$	$\frac{f(r)}{r}$	$\frac{g(r)}{r}$
.02	$2.383 \times 10^{-3}$	$5.985 \times 10^{-3}$	$4.014 \times 10^{-5}$	$-4.454 \times 10^{-6}$	$8.391 \times 10^{-4}$	$2.107 \times 10^{-3}$	$8.491 \times 10^{-3}$	$-2.090 \times 10^{-3}$	$1.582 \times 10^{-7}$	$1.329 \times 10^{-6}$
.12	1.678	3.970	$2.004 \times 10^{-4}$	$-3.040 \times 10^{-5}$	5.908	1.398	5.782	-1.915	$1.339 \times 10^{-6}$	$6.675 \times 10^{-6}$
.32	1.739	3.000	4.608	-7.035	6.122	1.056	4.146	-1.459	4.416	$1.555 \times 10^{-5}$
.62	1.920	2.300	7.678	$-1.184 \times 10^{-4}$	6.761	$8.101 \times 10^{-4}$	2.889	-1.111	$1.088 \times 10^{-5}$	2.643
1.42	2.177	1.329	$1.272 \times 10^{-3}$	-2.022	7.667	4.146	1.137	$-6.232 \times 10^{-4}$	3.568	4.641
2.40	2.116	$7.010 \times 10^{-4}$	1.491	-2.483	7.452	2.469	$1.178 \times 10^{-4}$	-3.113	7.335	5.913
4.40	1.438	1.170	1.272	-2.431	5.492	$4.119 \times 10^{-5}$	-5.188	-3.300	$1.479 \times 10^{-4}$	6.307
6.40	$6.498 \times 10^{-4}$	$-7.624 \times 10^{-5}$	$7.541 \times 10^{-4}$	-1.862	2.288	-2.686	-4.468	$4.905 \times 10^{-5}$	1.988	5.373
8.40	$3.484 \times 10^{-5}$	$-1.181 \times 10^{-4}$	2.579	-1.223	$1.221 \times 10^{-5}$	-4.159	-2.095	5.933	2.212	4.072
10.40	$-3.545 \times 10^{-4}$	-1.029	-1.120	$-6.774 \times 10^{-5}$	$-1.249 \times 10^{-4}$	-3.623	$8.735 \times 10^{-6}$	4.549	2.192	2.812
12.40	-5.474	$-7.090 \times 10^{-5}$	-3.412	-2.690	-1.928	-2.496	$1.557 \times 10^{-4}$	2.674	1.999	1.748
14.40	-5.949	-3.882	-4.501	$8.953 \times 10^{-7}$	-2.045	-1.366	2.296	1.035	1.698	$9.173 \times 10^{-6}$
18.40	-4.428	$6.076 \times 10^{-6}$	-4.693	$1.802 \times 10^{-5}$	-1.559	$2.152 \times 10^{-6}$	2.224	$-9.239 \times 10^{-6}$	$9.727 \times 10^{-5}$	-1.242
24.00	$-7.630 \times 10^{-5}$	$2.738 \times 10^{-5}$	-1.759	2.833	$-2.673 \times 10^{-5}$	9.650	$7.174 \times 10^{-5}$	$-1.448 \times 10^{-5}$	$5.380 \times 10^{-6}$	-6.513
44.00	$2.924 \times 10^{-4}$	$5.932 \times 10^{-7}$	2.646	$-4.910 \times 10^{-6}$	$1.028 \times 10^{-4}$	$1.943 \times 10^{-7}$	$-1.331 \times 10^{-4}$	$2.688 \times 10^{-6}$	$-8.549 \times 10^{-5}$	-2.090
64.00	$-2.830 \times 10^{-5}$	$-7.414 \times 10^{-6}$	$4.584 \times 10^{-5}$	-6.436	$-1.038 \times 10^{-5}$	$-2.617 \times 10^{-6}$	$2.078 \times 10^{-5}$	3.321	-2.523	1.021
84.00	$-2.000 \times 10^{-4}$	-4.208	$-1.308 \times 10^{-4}$	-1.843	-7.059	-1.472	9.622	$5.844 \times 10^{-7}$	2.586	1.371
120.00	-1.161	$4.658 \times 10^{-7}$	-1.616	1.631	-5.575	$1.881 \times 10^{-7}$	5.576	$-1.094 \times 10^{-6}$	5.549	$7.503 \times 10^{-7}$
220.00	1.172	$1.125 \times 10^{-6}$	$6.475 \times 10^{-5}$	$5.257 \times 10^{-7}$	4.251	3.866	-6.797	$-8.433 \times 10^{-8}$	2.296	$-3.148 \times 10^{-8}$
320.00	1.497	$3.754 \times 10^{-7}$	$1.230 \times 10^{-4}$	-1.560	4.866	$8.494 \times 10^{-8}$	-4.468	$2.076 \times 10^{-7}$	$-5.243 \times 10^{-6}$	$-1.241 \times 10^{-7}$
420.00	1.174	$9.062 \times 10^{-8}$	1.107	-2.489	2.984	-3.331	$-5.083 \times 10^{-6}$	1.712	$-1.971 \times 10^{-5}$	-1.211
620.00	$5.470 \times 10^{-5}$	-4.168	$6.172 \times 10^{-5}$	-1.546	$-5.002 \times 10^{-6}$	-7.184	$3.604 \times 10^{-5}$	$4.523 \times 10^{-8}$	-3.048	$-8.423 \times 10^{-8}$
820.00	2.313	-2.271	3.007	$-7.456 \times 10^{-8}$	$-2.191 \times 10^{-5}$	-5.060	4.121	$-9.513 \times 10^{-9}$	-3.144	-5.262
1020.00	$9.481 \times 10^{-6}$	-1.205	1.400	-5.061	-2.651	-2.763	3.375	$-2.372 \times 10^{-8}$	-2.804	-3.074
1420.00	1.531	$-2.444 \times 10^{-9}$	$2.852 \times 10^{-6}$	$-6.770 \times 10^{-9}$	-2.074	$-3.184 \times 10^{-9}$	1.617	-1.735	-1.865	$-8.203 \times 10^{-9}$
1820.00	$2.402 \times 10^{-7}$	$-4.271 \times 10^{-10}$	$3.188 \times 10^{-7}$	-1.300	-1.203	2.811	$6.387 \times 10^{-6}$	$-7.867 \times 10^{-9}$	-1.075	$-7.861 \times 10^{-10}$
2600.00	$6.195 \times 10^{-8}$	$-1.224 \times 10^{-11}$	$2.155 \times 10^{-8}$	$-4.915 \times 10^{-11}$	$-2.960 \times 10^{-6}$	1.777	$8.224 \times 10^{-7}$	-1.131	$-2.933 \times 10^{-6}$	9.397
3100.00	$5.710 \times 10^{-10}$	$-1.219 \times 10^{-12}$	$3.197 \times 10^{-9}$	$-4.917 \times 10^{-12}$	-1.067	$7.784 \times 10^{-10}$	2.025	$-2.884 \times 10^{-10}$	-1.160	5.451
3600.00					$-3.634 \times 10^{-7}$	2.984	$4.788 \times 10^{-8}$	$-6.975 \times 10^{-11}$	$-4.377 \times 10^{-7}$	2.529
4100.00					-1.189	1.058	1.109	-1.617	-1.593	1.051
4600.00					$-3.776 \times 10^{-8}$	$3.563 \times 10^{-11}$	$2.825 \times 10^{-9}$	$-3.256 \times 10^{-12}$	$-5.638 \times 10^{-8}$	$4.083 \times 10^{-11}$
5600.00					$-3.316 \times 10^{-9}$	$3.946 \times 10^{-12}$			$-6.639 \times 10^{-9}$	$5.435 \times 10^{-12}$
6600.00									$-7.359 \times 10^{-10}$	$6.509 \times 10^{-13}$

Table II.

Spectroscopic level designation	Fitted energy level (ionization energy, $m_e c^2=1$ )	Spectroscopic energy level <sup>a</sup>	Valence-electron hyperfine splitting (GHz)	Observed hyperfine splitting (GHz)
$6p^2P_{1/2}$	$1.1939 \times 10^{-5}$	$1.1953 \times 10^{-5}$	21.8	$21.3^b$
$6p^2P_{3/2}$	$9.8745 \times 10^{-6}$	$1.0062 \times 10^{-5}$	3.27	$.528^c$
$7p^2P_{1/2}$	$3.6756 \times 10^{-6}$	$3.6648 \times 10^{-6}$	2.71	$2.13^d$
$7p^2P_{3/2}$	$3.3937 \times 10^{-6}$	$3.4219 \times 10^{-6}$	.494	$.62^d$
$8p^2P_{1/2}$	$1.9199 \times 10^{-6}$	$1.9158 \times 10^{-6}$	.989	$.79^e$
$8p^2P_{3/2}$	$1.8155 \times 10^{-6}$	$1.8254 \times 10^{-6}$	.187	$.26^e$
$7s^2S_{1/2}$	$5.4164 \times 10^{-6}$	$5.5289 \times 10^{-6}$	14.3	$12.4^b$
$8s^2S_{1/2}$	$2.5169 \times 10^{-6}$	$2.5521 \times 10^{-6}$	4.32	
$9s^2S_{1/2}$	$1.4650 \times 10^{-6}$	$1.4796 \times 10^{-6}$	1.90	
$10s^2S_{1/2}$	$9.594 \times 10^{-7}$	$9.6260 \times 10^{-7}$	1.01	
$11s^2S_{1/2}$	$6.772 \times 10^{-7}$	$6.811 \times 10^{-7}$	0.59	

Table II References

- a) C.E. Moore, Atomic Energy Levels Vol. III, Circular of Nat. B. of Stand. 467 (1958).
- b) A. Gallagher and A. Lurio, Phys. Rev. 136, A87 (1964).
- c) G. Gould, Phys. Rev. 101, 1828 (1956).
- d) A. Flusberg, T. Mossberg and S.R. Hartmann, Phys. Lett. 55A, 403 (1976).
- e) A.N. Odintsov, Opt. i Spektr. 9, 75 (142), (1960).

Table III.

Transition	A-coefficient (Gallagher & Lurio) <sup>a</sup> 10 <sup>7</sup> sec <sup>-1</sup>	A-coefficient (this work) 10 <sup>7</sup> sec <sup>-1</sup>	Radial integral <r> <sub>fi</sub> (λ)	Oscillator strength (this work)	Oscillator strength (A,A,&T) <sup>b</sup>
7 <sup>2</sup> S <sub>1/2</sub> -6 <sup>2</sup> P <sub>1/2</sub>	6.25±0.31	5.78	294.1	.124	.123
8 <sup>2</sup> S <sub>1/2</sub> -6 <sup>2</sup> P <sub>1/2</sub>	1.78±0.16	1.75	91.5	.0175	.0172
9 <sup>2</sup> S <sub>1/2</sub> -6 <sup>2</sup> P <sub>1/2</sub>	.78±0.10	0.777	51.8	.00625	.00616
10 <sup>2</sup> S <sub>1/2</sub> -6 <sup>2</sup> P <sub>1/2</sub>	---	0.412	35.1	.00301	.00295
11 <sup>2</sup> S <sub>1/2</sub> -6 <sup>2</sup> P <sub>1/2</sub>	.31±0.06	0.244	26.0	.00170	.00167
7 <sup>2</sup> S <sub>1/2</sub> -6 <sup>2</sup> P <sub>3/2</sub>	7.05±0.32	8.30	422.1	.178	.162
8 <sup>2</sup> S <sub>1/2</sub> -6 <sup>2</sup> P <sub>3/2</sub>	1.73±0.18	2.30	103.9	.0180	.0172
9 <sup>2</sup> S <sub>1/2</sub> -6 <sup>2</sup> P <sub>3/2</sub>	0.80±0.08	1.01	56.3	.00605	.0059
10 <sup>2</sup> S <sub>1/2</sub> -6 <sup>2</sup> P <sub>3/2</sub>	0.57±0.06	.534	37.5	.00285	.00286
6 <sup>2</sup> D <sub>3/2</sub> -6 <sup>2</sup> P <sub>1/2</sub>	12.6 ±1.0	16.04	-307.7	.368	.40
7 <sup>2</sup> D <sub>3/2</sub> -6 <sup>2</sup> P <sub>1/2</sub>	4.4 ±0.5	6.39	-154.8	.109	.121
8 <sup>2</sup> D <sub>3/2</sub> -6 <sup>2</sup> P <sub>1/2</sub>	1.89±0.3	3.19	- 99.8	.0434	.053
9 <sup>2</sup> D <sub>3/2</sub> -6 <sup>2</sup> P <sub>1/2</sub>	.98±0.22	1.82	- 71.9	.0257	.028
10 <sup>2</sup> D <sub>3/2</sub> -6 <sup>2</sup> P <sub>1/2</sub>	.58±0.15	1.14	- 55.2	.0156	.017
6 <sup>2</sup> D <sub>3/2</sub> -6 <sup>2</sup> P <sub>3/2</sub>	2.20±0.23	2.88	-419.6	.0538	.052
7 <sup>2</sup> D <sub>3/2</sub> -6 <sup>2</sup> P <sub>3/2</sub>	0.76±0.08	1.01	-186.9	.0129	.0136
8 <sup>2</sup> D <sub>3/2</sub> -6 <sup>2</sup> P <sub>3/2</sub>	0.37±0.04	0.498	-117.5	.00549	.0056
9 <sup>2</sup> D <sub>3/2</sub> -6 <sup>2</sup> P <sub>3/2</sub>	0.19±0.02	0.279	- 83.0	.00285	.0029
6 <sup>2</sup> D <sub>5/2</sub> -6 <sup>2</sup> P <sub>3/2</sub>	12.4 ±1.5	16.3	-405.6	.489	.46
7 <sup>2</sup> D <sub>5/2</sub> -6 <sup>2</sup> P <sub>3/2</sub>	4.2 ±0.5	6.06	-186.9	.116	.12
8 <sup>2</sup> D <sub>5/2</sub> -6 <sup>2</sup> P <sub>3/2</sub>	1.7 ±0.2	2.96	-116.9	.0489	.051

<sup>a</sup>Ref. 11

<sup>b</sup>Ref. 12

Table IV.

Transition	Radial integral <r>pi ( $\lambda$ )	Oscillator strength (this work)	Oscillator strength <sup>12</sup> (A, A & T)
$7^2S_{1/2} - 7^2P_{1/2}$	-1072.6	.315	.440
$8^2S_{1/2} - 7^2P_{1/2}$	991.6	.241	.258
$9^2S_{1/2} - 7^2P_{1/2}$	219.5	.0234	.0219
$10^2S_{1/2} - 7^2P_{1/2}$	114.3	.00784	.00741
$11^2S_{1/2} - 7^2P_{1/2}$	75.1	.00277	.00342
$7^2S_{1/2} - 7^2P_{3/2}$	-1007.8	.476	.440
$8^2P_{1/2} - 7^2P_{3/2}$	1240.2	.297	.294
$9^2S_{1/2} - 7^2P_{3/2}$	202.2	.0176	.0164
$10^2S_{1/2} - 7^2P_{3/2}$	100.4	.00550	.00542
$6^2D_{3/2} - 7^2P_{1/2}$	1321.4	.369	.340
$7^2D_{3/2} - 7^2P_{1/2}$	- 489.2	.202	.248
$8^2D_{3/2} - 7^2P_{1/2}$	- 254.2	.0733	.0850
$9^2D_{3/2} - 7^2P_{1/2}$	- 165.3	.0352	.0399
$10^2D_{3/2} - 7^2P_{1/2}$	- 120.0	.0199	.0223
$6^2D_{3/2} - 7^2P_{3/2}$	1328.0	.0152	.0166
$7^2P_{3/2} - 7^2P_{3/2}$	- 729.8	.0396	.0418
$8^2D_{3/2} - 7^2P_{3/2}$	- 331.0	.00937	.0116
$9^2D_{3/2} - 7^2P_{3/2}$	- 204.9	.00495	.00506



Table V. g-factor anomaly calculation and comparison with experiment.

---

Measured $6^2P_{1/2}$ g-factor	.6656924 (18) <sup>a</sup>
0-order theory	.6658936
g-factor anomaly	- .0002012 (18) <sup>a</sup>
calculated anomaly	
relativistic	- .000107
configuration interaction	< .000001
Lamb	- .000006
orbit-orbit	- .000082
	<hr/>
Total calculated anomaly	- .000195

---

<sup>a</sup>Ref. 19.

Table VI

Transition	$\mathcal{M} \times 3/\sqrt{2}$	$A_{M1} (\text{sec}^{-1})$	$\int_0^\infty f_f r^2 f_{\frac{1}{2}} dr,$ ( $\lambda^2$ )	$A_{E2} (\text{sec}^{-1})$
$6^2P_{\frac{1}{2}} - 6^2P_{3/2}$	+ .9796	4.083	$2.94 \cdot 10^5$	.158
$6^2P_{\frac{1}{2}} - 7^2P_{3/2}$	- .0902	3.31	$-1.27 \cdot 10^5$	55.2
$7^2P_{\frac{1}{2}} - 6^2P_{3/2}$	- .115	2.18	$-3.00 \cdot 10^5$	72.8
$7^2P_{\frac{1}{2}} - 7^2P_{3/2}$	+ .9822	$8.706 \cdot 10^{-3}$	$2.40 \cdot 10^6$	$3.69 \cdot 10^{-4}$

Table VII. Calculation of  $\epsilon_{PV}$

Intermediate s-state	Contributions to $\epsilon_{PV}$	
	$\frac{\langle 7P_{\frac{1}{2}}   E1   ns \rangle \langle ns   H_{PV}   6P_{\frac{1}{2}} \rangle}{E_6 - E_n}$	$\frac{\langle 7P_{\frac{1}{2}}   H_{PV}   ns \rangle \langle ns   E1   6P_{\frac{1}{2}} \rangle}{E_7 - E_n}$
6s >	$-i 0.197 \cdot 10^{-10} Q_w  \mu_B $	$+i 0.631 \cdot 10^{-10} Q_w  \mu_B $
7s >	$+i 5.08$	$-i 1.69$
8s >	$-i 1.77$	$+i 0.485$
9s >	$-i 0.232$	$+i 0.093$
10s >	$-i 0.084$	$+i 0.037$
Total	$i 2.81 \cdot 10^{-10} Q_w  \mu_B $ $= i 2.36 \cdot 10^{-10} Q_w  \mu_B $	$-i 0.45 \cdot 10^{-10} Q_w  \mu_B $
Method B:	$i 2.13 \cdot 10^{-10} Q_w  \mu_B $ $= i 1.93 \cdot 10^{-10} Q_w  \mu_B $	$-i 0.20 \cdot 10^{-10} Q_w  \mu_B $

Table VIII.  $\epsilon_{PV}$  for  $n'P_{1/2} - nP_{3/2}$  transitions.

Method 1: 
$$\sum \frac{e \langle nP_{3/2} | E | ns \rangle \langle ns | H_{PV} | n'P_{1/2} \rangle}{E_{P_{1/2}} - E_s}$$

Intermediate s-state	$6^2P_{3/2} - 6^2P_{1/2}$	$7^2P_{3/2} - 6^2P_{1/2}$	$6^2P_{3/2} - 7^2P_{1/2}$
6s>	-i 4.22 × 10 <sup>-10</sup> Q <sub>w</sub>  μ <sub>B</sub>	-i 0.65	-i 0.86
7s>	-i 2.83	+i 6.76	+i 3.43
8s>	-i 0.264	-i 3.13	-i 0.78
9s>	-i 0.041	-i 0.30	-i 0.14
10s>	-i 0.041	-i 0.10	-i 0.06
Total	-i 7.45 × 10 <sup>-10</sup> Q <sub>w</sub>  μ <sub>B</sub>	+i 2.58	+i 1.58
Method 2:	-i 8.09 × 10 <sup>-10</sup> Q <sub>w</sub>  μ <sub>B</sub>	+i 1.75 × 10 <sup>-10</sup> Q <sub>w</sub>  μ <sub>B</sub>	+i 1.25 × 10 <sup>-10</sup> Q <sub>w</sub>  μ <sub>B</sub>

Table IX

Quantity Summed	Finite sum over 5 lowest energy levels ( $7^2S_{1/2} - 11^2S_{1/2}, 6^2D_{3/2} - 10^2D_{3/2}$ )	Green's function method
$\frac{R_{7P,nS} R_{nS,6P}}{E_6 - E_{nS}}$	$3.78 \cdot 10^{10}$	$3.64 \cdot 10^{10}$
$\frac{R_{7P,nS} R_{nS,6P}}{E_7 - E_{nS}}$	$-2.58 \cdot 10^{11}$	$-2.71 \cdot 10^{11}$
$\frac{R_{7P,nD} R_{nD,6P}}{E_6 - E_{nD}}$	$3.50 \cdot 10^{10}$	$2.81 \cdot 10^{10}$
$\frac{R_{7P,nD} R_{nD,6P}}{E_7 - E_{nD}}$	$8.00 \cdot 10^{11}$	$7.01 \cdot 10^{11}$
$e^2 \alpha$ (in units $\frac{\mu_B}{\text{volts/cm}}$ )	$2.43 \cdot 10^{-5}$	$2.05 \cdot 10^{-5}$
$e^2 \beta$	$1.78 \cdot 10^{-5}$	$1.64 \cdot 10^{-5}$
$\beta/\alpha$	.73	.80

Table X. Dipole transition amplitudes  $D = \langle M1 \rangle + \langle E1_{PV} \rangle + \langle E1_{STARK} \rangle$   
for  $6^2P_{1/2} (F, m_F) \rightarrow 7^2P_{1/2} (F', m_{F'})$  transitions.

		$6^2P_{1/2}, F, m_F$			
		0	1	1	1
$7^2P_{1/2}, F', m_{F'}$	0 0	$\alpha' \cos\theta$	$\frac{i}{\sqrt{2}}(\mathcal{M} \sin\theta - \beta' \sin\theta + \mathcal{E}_{PV} \cos\theta)$	$-\mathcal{M} \cos\theta + \mathcal{E}_{PV} \sin\theta$	$\frac{i}{\sqrt{2}}(\mathcal{M} \sin\theta + \beta' \sin\theta + \mathcal{E}_{PV} \cos\theta)$
	1 -1	$\frac{i}{\sqrt{2}}(-\mathcal{M} \sin\theta - \beta' \sin\theta - \mathcal{E}_{PV} \cos\theta)$	$\alpha' \cos\theta - \mathcal{M} \cos\theta + \mathcal{E}_{PV} \sin\theta$	$\frac{i}{\sqrt{2}}(\mathcal{M} \sin\theta + \beta' \sin\theta + \mathcal{E}_{PV} \cos\theta)$	0
	1 0	$-\mathcal{M} \cos\theta$	$\frac{i}{2}(\mathcal{M} \sin\theta - \beta' \sin\theta + \mathcal{E}_{PV} \cos\theta)$	$\alpha' \cos\theta$	$\frac{-i}{2}(\mathcal{M} \sin\theta + \beta' \sin\theta + \mathcal{E}_{PV} \cos\theta)$
	1 1	$\frac{i}{\sqrt{2}}(-\mathcal{M} \sin\theta + \beta' \sin\theta - \mathcal{E}_{PV} \cos\theta)$	0	$\frac{i}{\sqrt{2}}(\mathcal{M} \sin\theta - \beta' \sin\theta + \mathcal{E}_{PV} \cos\theta)$	$\alpha' \cos\theta + \mathcal{M} \cos\theta - \mathcal{E}_{PV} \sin\theta$

$$\alpha' = e^2 E_0 \alpha$$

$$\beta' = e^2 E_0 \beta$$

Table XI.  $P_{3/2} - P_{1/2}$  transition amplitudes.

$m_{P_{3/2}} \backslash m_{P_{1/2}}$	$\frac{1}{2}$	$-\frac{1}{2}$
$\frac{3}{2}$	$\left(\frac{\sqrt{3}}{2} \mathcal{M} + \frac{\mathcal{E}_2}{\sqrt{6}}\right) i \sin\theta$ $+ i \frac{\sqrt{3}}{2} \mathcal{E}_{PV} \cos\theta$	$-\sqrt{\frac{2}{3}} \mathcal{E}_2 \cos\theta$
$\frac{1}{2}$	$\mathcal{M} \cos\theta + \mathcal{E}_{PV} \sin\theta$	$\left(\frac{\mathcal{M}}{2} - \frac{\mathcal{E}_2}{\sqrt{2}}\right) i \sin\theta$ $+ i \frac{\mathcal{E}_{PV}}{2} \cos\theta$
$-\frac{1}{2}$	$\left(\frac{\mathcal{M}}{2} - \frac{\mathcal{E}_2}{\sqrt{2}}\right) i \sin\theta$ $+ i \frac{\mathcal{E}_{PV}}{2} \cos\theta$	$-\mathcal{M} \cos\theta + \mathcal{E}_{PV} \sin\theta$
$-\frac{3}{2}$	$-\sqrt{\frac{2}{3}} \mathcal{E}_2 \cos\theta$	$\left(\frac{\sqrt{3}}{2} \mathcal{M} + \frac{\mathcal{E}_2}{\sqrt{6}}\right) i \sin\theta$ $+ i \frac{\sqrt{3}}{2} \mathcal{E}_{PV} \cos\theta$

Table XII. Amplitudes for  $P_{3/2}-P_{1/2}$  transitions.

Transition amplitude	$6P_{3/2}-6P_{1/2}$	$7P_{3/2}-7P_{1/2}$	$6P_{3/2}-7P_{1/2}$
$\mathcal{M}$	$.98 \frac{\sqrt{2}}{3}$	$-.092 \frac{\sqrt{2}}{3}$	$-.115 \frac{\sqrt{2}}{3}$
$\epsilon_2$	.22	-.434	.767
$\epsilon_{PV}$	$-i 8.09 \times 10^{-10} Q_w$	$+i 1.75 \times 10^{-10} Q_w$	$+i 1.26 \times 10^{-10} Q_w$
$P(Q_w = -140)$	$4.17 \times 10^{-7}$	$1.67 \times 10^{-8}$	$4.85 \times 10^{-9}$

$$\mathcal{M} = \frac{-\sqrt{2}}{\omega} \int (f_{1/2} g_{3/2} + g_{1/2} f_{3/2}) g_1(\omega r) dr \quad |\mu_B|$$

$$\epsilon_2 = \frac{2\omega}{5} \int f_{1/2} f_{3/2} r^2 dr \quad |\mu_B|$$

$$\epsilon_{PV} = \frac{2\sqrt{2}}{3} \sum \frac{\langle P_{3/2} | r | ns \rangle \langle ns | H_{PV} | P_{1/2} \rangle}{E_{1/2} - E_n} \quad |\mu_B|$$



This report was done with support from the United States Energy Research and Development Administration. Any conclusions or opinions expressed in this report represent solely those of the author(s) and not necessarily those of The Regents of the University of California, the Lawrence Berkeley Laboratory or the United States Energy Research and Development Administration.

TECHNICAL INFORMATION DIVISION  
LAWRENCE BERKELEY LABORATORY  
UNIVERSITY OF CALIFORNIA  
BERKELEY, CALIFORNIA 94720